Tampere University

Riikka Järvinen

CHARACTERIZATION AND OPTIMIZATION OF AN OPTOGENETIC LEXY SWITCH FOR STUDYING NUCLEOCYTOPLASMIC TRANSPORT IN EPITHELIAL CELLS

Faculty of Medicine and Health Technology
Master's Thesis
November 24

ABSTRACT

Riikka Järvinen: Characterization and Optimization of an Optogenetic LEXY Switch for Studying Nucleocytoplasmic Transport in Epithelial Cells
Master's thesis
Tampere University
Master's degree Programme in Biotechnology and Biomedical Engineering
Supervisors: Bobin George Abraham and Teemu Ihalainen
Examiners: Heli Skottman and Teemu Ihalainen
November 2024

This master's thesis explores the impact of mechanical perturbations on nucleocytoplasmic transport (NCT) in epithelial cells by employing the optogenetic LEXY system, a light-controlled construct that enables dynamic regulation of protein movement between the nucleus and cytoplasm. Cellular responses to mechanical signals play a vital role in regulating essential processes such as gene expression, cell division, and differentiation. The nucleus acts as a mechanosensor, responding to forces exerted on the cell. However, the precise mechanisms by which mechanical stimuli influence NCT, are not fully understood.

In this study, MDCK II and MCF7 epithelial cell lines were genetically modified to stably express the LEXY system, facilitating real-time monitoring of nuclear protein export and import in response to blue light stimulation. Using a confocal microscope, cells were observed in a series of experimental setups where they were subjected to light-induced activations under controlled, cytoskeleton-disrupted, and compressed conditions. In MDCK II cells, mechanical compression increased the rate of nuclear import, suggesting that physical deformation may alter nuclear envelope tension and nuclear pore complex dynamics to facilitate transport. In contrast, cytoskeletal disruption, induced through actin and microtubule destabilization, resulted in slower NCT rates, indicating the essential role of cytoskeletal integrity in maintaining efficient transport pathways.

The breast cancer cell line MCF-7, exhibited minimal changes in NCT rates under mechanical perturbations, indicating that cancer-like nuclei might be less sensitive to mechanical stimuli or may possess adaptive mechanisms that sustain transport efficiency. These results highlight cell-specific variations in mechanotransduction, emphasizing that while the nucleus in epithelial cells generally serves as a mechanosensitive organelle, the degree of sensitivity and the nuclear response can vary significantly with cellular context and structural properties. This work provides new insights into the role of nuclear mechanics in cellular adaptation to physical stimuli, contributing to our understanding of mechanotransduction pathways.

Keywords: optogenetics, mechanotransduction, NTC, epithelial cell

TIIVISTELMÄ

Riikka Järvinen: Optogeneettisen LEXY-työkalun karakterisointi ja optimointi tumakuljetuksen tutkimiseksi epiteelisoluissa
Pro Gradu -tutkielma
Tampereen yliopisto
Bioteknologian ja biolääketieteen tekniikan maisteriohjelma
Ohjaajat: Bobin George Abraham ja Teemu Ihalainen
Tarkastajat: Heli Skottman ja Teemu Ihalainen
Marraskuu 2024

Tässä pro gradu -tutkielmassa tutkittiin mekaanisten häiriöiden vaikutusta tumakuljetukseen epiteelisoluissa. Tutkimus tehtiin hyödyntämällä optogeneettistä LEXY-työkalua, valolla säädeltävää konstruktiota, joka mahdollistaa proteiinien liikkeen ohjaamisen tuman ja sytoplasman välillä. Solujen vasteet mekaanisiin signaaleihin ovat keskeisiä elintärkeiden prosessien, kuten geenien ekspression, solunjakautumisen ja erilaistumisen säätelyssä. Tuma toimii mekaanisena sensorina, joka reagoi soluun kohdistuviin voimiin. Tarkat mekanismit, joilla mekaaniset ärsykkeet vaikuttavat tumakuljetusprosessiin, eivät ole täysin ymmärrettyjä.

Tutkimuksessa käytettiin MDCK II ja MCF-7 epiteelisolulinjoja, joita muokattiin geneettisesti ilmentämään pysyvästi fluoresoivalla merkkiaineella yhdistettyä LEXY-järjestelmää. Tämä mahdollisti tumaproteiinien liikkeen reaaliaikaisen seurannan vasteena sinivalostimulaatioon. Konfokaalimikroskooppia käyttäen solujen vastetta sinivaloaktivaatiolle tutkittiin kontrollisolujen lisäksi tilanteissa, joissa solun tukiranka oli hajotettu tai soluihin kohdistettiin mekaanista puristusta. MDCK II -soluissa mekaaninen puristus nopeutti konstruktion kulkeutumista tumaan, mikä viitannee siihen, että tumaan kohdistettava voima saattaa muuttaa tumakalvon jännitystä ja tumakuljetuksen dynamiikkaa. Sen sijaan solutukirangan hajottaminen hidasti tumakuljetusprosessia, mikä osoittaa solutukirangan tärkeyden tehokkaan tumakuljetuksen ylläpitämisessä.

Rintasyöpäsoluissa (MCF-7), joiden tumat ovat usein hyvin muovautuvia, tumakuljetuksen nopeuden muutoksia havaittiin vain vähän. Tämä viitannee siihen, että syöpäsolujen tumat olisivat vähemmän herkkiä mekaanisille ärsykkeille, tai että muut mekanismit ovat tärkeämmässä roolissa tumakuljetuksen säätelyssä. Tulokset korostavat solukohtaisia eroja ja osoittavat, että vaikka tuma epiteelisoluissa yleensä toimii mekaanisena sensorina, herkkyyden aste ja tuman vaste voivat vaihdella merkittävästi solukontekstin ja rakenteellisten ominaisuuksien mukaan. Tämä työ tarjoaa uutta tietoa tuman mekaanisten ominaisuuksien roolista solujen sopeutumisessa mekaanisiin ärsykkeisiin, mikä syventää ymmärrystämme mekanobiologisista signalointireiteistä.

Avainsanat: optogenetiikka, mekanotransduktio, tumakuljetus, epiteelisolu

The AI tools used in my thesis and the purpose of their use has been described below:

ChatGPT-4

Purpose of use and the part in which it was used: proofreading of the written text.

I am aware that I am totally responsible for the entire content of the thesis, including the parts generated by AI, and accept the responsibility for any violations of the ethical standards of publications.

PREFACE

This master's thesis was performed in Cellular Biophysics research group. I want to thank both my supervisors Bobin George Abraham and Teemu Ihalainen for introducing me to the field of optogenetics and for their invaluable support and guidance throughout this project. I would also like to thank all members of the Cellular Biophysics and Biophysics of the Eye groups, especially Anni Pörsti and Peppi Tolonen for peer support and the many insightful, late-night discussions we shared both in the lab and over coffee.

Lastly, I want to thank my family and friends for their support.

Tampere, 11th of November 2024

Riikka Järvinen

CONTENTS

1. INTRODUCTION 1
2. LITERATURE REVIEW 3
2.1 Nucleus and nuclear transport 3
2.1.1 Nuclear Pore Complex (NPC) 3
2.1.2 Nucleocytoplasmic transport 5
2.1.3 Regulation of nucleocytoplasmic transport 6
2.2 Cellular responses to external mechanical stimuli 8
2.2.1 Mechanosensing at adhesion sites 9
2.2.2 Force propagation through the cytoskeleton to the nucleus 10
2.2.3 Nucleus as a mechanosensor 11
2.3 Optogenetics 13
2.3.1 Light-inducible nuclear export system (LEXY) 15
3. AIMS OF THE STUDY 17
4. MATERIALS AND METHODS 18
4.1 Cell lines 18
4.2 Transient transfection with Fugene HD 18
4.3 Stable cell line generation 18
4.3.1 Transfection with Neon electroporation system 18
4.3.2 Fluorescence-activated cell soring (FACS) 19
4.4 Cytoskeletal disruption by cytochalasin D and nocodazole 20
4.5 Polyacrylamide gel cushions 20
4.5.1 Coverslip cleaning and activation 20
4.5.2 Polyacrylamide gel preparation 20
4.6 Immunostaining 21
4.6.1 Microscopy 21
4.7 Live-cell imaging 22
4.7.1 Single-cell activations 22
4.7.2 Whole-field-of-view activations 22
4.8 Image analysis 23
4.8.1 Curve fitting 23
4.8.2 Statistical analysis 24
5. RESULTS 25
5.1 Setting up the LEXY system 25
5.2 Whole-field-ofview stimulations of MDCK II-LEXY cells after cytoskeleton disruption/perturbation 28
5.3 Whole-field-of-view stimulations of MDCK II-LEXY cells after compression 29
5.4 Whole-field-of-view stimulations of MCF7-LEXY cells 32
5.5 N/C ratios in the dark state 35
5.6 Curve fitting and kinetic analysis 36

6. DISCUSSION 40
6.1 LEXY's performance 40
6.2 Single-cell vs whole-field-of-view activations 41
6.3 Nuclear compression appears to accelerates import, while cytoskeletal disruption slows it in MDCK II cells 42
6.4 Mechanical perturbations do not directly affect import rates in MCF7 cells 44
6.5 Sources of error and limitations of the study 45
7. CONCLUSIONS 47
REFERENCES 49

LIST OF SYMBOLS AND ABBREVIATIONS

AJ	Adherens junction
AsLOV2	Avena sativa LOV2 domain
CRM1	Chromosomal Maintenance 1
ECM	Extracellular matrix
FA	Focal adhesion
FG-Nup	Phenylalanine-glycine rich nucleoporin
GDP	Guanosine diphosphate
GTP	Guanosine triphosphate
INM	Inner nuclear membrane
KASH	Klarsicht, ANC-1, Syne Homology
LEXY	Light-inducible Nuclear Export System
LINC	Linker of nucleoskeleton and cytoskeleton
MCF7	Michigan Cancer Foundation-7
MDCK II	Madin-Darby canine kidney II
NCT	Nucleocytoplasmic transport
NES	Nuclear export signal
NLS	Nuclear localization signal
NPC	Nuclear pore complex
NTR	Nuclear transport receptor
ONM	Outer nuclear membrane
POI	Protein of interest
Ran	Ras-related nuclear protein
SUN	Sad1, UNC-84

1. INTRODUCTION

Cells are in constant communication with their surroundings, responding to both chemical and mechanical signals from the extracellular matrix (ECM) and adjacent cells. This phenomenon, known as mechanosensing, allows cells to detect external forces such as tension and shear, which they convert into biological responses through a process called mechanotransduction. Mechanical signals travel from the ECM through the cell membrane connections and along the actin cytoskeleton to the nucleus. These mechanical signals propagate faster than biochemical signals, yet they can produce similar effects, particularly in epithelial tissues with strong cell–cell adhesion[1]. While it is well-established that mechanosensing at the plasma membrane plays a crucial role in mechanotransduction, recent insights suggest that the nucleus itself may also serve as a mechanosensitive structure. Moreover, the nucleus can alter its mechanical properties, such as stiffness and shape, in reaction to external forces.

The interplay between mechanosensing, mechanotransduction, and protein transport across the nuclear envelope is interconnected. This allows cells to respond to mechanical cues by modifying the transport of proteins across the nuclear envelope, which is vital for cellular adaptation, survival, and function. All protein trafficking through the nuclear envelope is facilitated by the nuclear pore complex (NPC), a large and intricately structured protein assembly that spans the nuclear membrane and permits rapid transport of up to 1000 molecules per second[2,3]. Overall, the relationship between mechanical changes in the nucleus and nucleocytoplasmic transport is complex, involving alterations in nuclear structure, NPC dynamics, mechanosensitive proteins, and signalling pathways.

Given that protein transport is highly regulated both spatially and temporally, studying these dynamic processes presents certain challenges. A groundbreaking approach in this area is optogenetics, which merges genetic engineering with light exposure to precisely control the activity of specific proteins in living cells[4]. This technique has proven to be increasingly useful for investigating protein transport, particularly in mammalian cells, as it allows for dynamic and reversible manipulation of cellular functions. A significant tool in this field is the Light-inducible Nuclear Export System (LEXY), which utilizes the AsLOV2 domain derived from Avena sativa (oat) to regulate the export of proteins from

the nucleus in response to blue light[5]. When exposed to light, LEXY reveals a nuclear export signal, enabling tagged proteins to exit the nucleus and return once the light is turned off.

The reversible functionality of LEXY enables high-resolution investigations of nucleo-cytoplasmic transport and cellular responses to mechanical changes. The objective of this master's thesis is to set up the LEXY imaging system at the Tampere imaging facility and use it to study nucleocytoplasmic transport when the mechanical properties of the nucleus are modified in epithelial cells.

2. LITERATURE REVIEW

2.1 Nucleus and nuclear transport

In eukaryotic cells, the nucleus is surrounded by the nuclear envelope. This double lipid membrane separates the nucleus from the cytoplasm protecting the DNA in the nucleus. While a high level of subcellular compartmentalization is a hallmark of eukaryotic cells, this adds some logistic challenges in transporting molecules to their destination compartments. Processes essential for cellular viability, such as cell growth, gene expression and cell division, are dependable on continuous trafficking of molecules such as proteins, RNA and metabolites across the nuclear membrane[6,7]. This bidirectional nucleocytoplasmic exchange of molecules is facilitated by a single versatile channel called the nuclear pore complex (NPC). Each of these complexes are known to facilitate the transportation of up to 1000 molecules per second[2,3].

As efficient nucleocytoplasmic transportation is crucial for cell homeostasis, dysfunction of this system is known to cause disease and affect aging[8,9]. Disruptions of the NPC, altered nucleocytoplasmic transport and aberrant localization of misfolded proteins have been implicated in the pathophysiology of several neurodegenerative diseases including Alzheimer's disease, amyotrophic lateral sclerosis, and frontotemporal dementia[6,7]. Aberrant protein localization is a prominent feature in diverse array of human diseases, including cancer. For example, in cancer cells, aberrant cytoplasmic sequestration of tumor suppressor transcription as well as localization of oncoproteins in the nucleus can result in their respective inactivation or over-activation[8,12].

2.1.1 Nuclear Pore Complex (NPC)

Nuclear pore complexes are large macromolecules which are embedded in the nuclear envelope. NPCs fuse the inner (INM) and outer (ONM) nuclear membranes to form an approx. 40-70 nm wide channel[13,14]. NPCs are large (90–120 MDa)[15] octagonal structures, composed of multiple copies of around 30 different nuclear pore proteins called nucleoporins (Nups). Each NPC is composed of approximately 500–1000 Nups, which makes them the largest protein complexes found in eucaryotic cells[15,16]. The number of NPCs is usually approx. 3000 – 5000 per mammalian cell nucleus, but this number varies by cell type and life cycle stage[16]. NPCs are shown to exhibit high plasticity in both their structure and function even within single cells[14,17].

Nevertheless, the main structure of NPC and most of its proteins are evolutionally highly conserved among eukaryotes and their structure have been intensively studied[18,19]. Integration of structural information from crystallography and mass spectrometry, high-resolution cryo-electron microscopy and recent AI-based structure predictions have provided detailed information about NPC structure and its assembly[19–21]. In brief, the structure of the NPC can be described as an eight-fold symmetrical structure containing three rings: the inner pore ring and the nuclear and cytoplasmic rings. In addition, the nuclear and cytoplasmic rings carry specialized attachments called the nuclear basket and the cytoplasmic filaments[16] (Fig 1). The central channel of NPC is filled with disordered phenylalanine-glycine (FG)-rich Nups, and these FG-repeats are found in approximately one-third of all Nups[7]. FG-Nups play a crucial role in the structure and function of the NPC and form a selective permeability barrier within the pore[7]. Whereas the majority of the FG-Nups reside in the central channel, some of these also reach into the nucleoplasm and cytoplasm sides[16]. In addition to their main function as mediators of nucleocytoplasmic transport, NPCs have important transport-independent roles. NPC components are shown to have both direct and indirect interactions with cyto- and nucleoskeleton[22]. There is also accumulating evidence that specific FG-Nups of the nuclear basket can interact with chromatin and thus possibly influence chromatin organization and transcription[23,24].

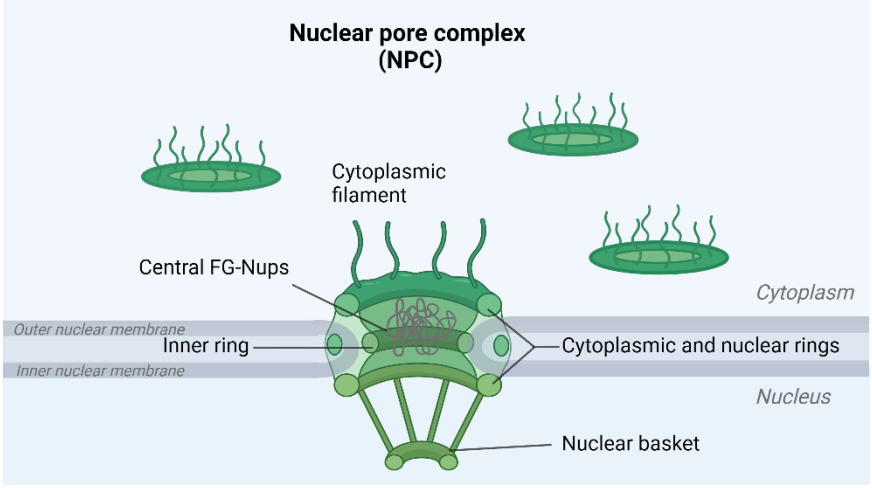

Figure 1 Cross-section of the NPC showing the major structural features. The NPC is composed of cytoplasmic and nuclear rings and the inner ring. Eight filaments project from the NPC into the cytoplasm while eight nuclear filaments are joined in a distal ring and form the nuclear basket. FG-Nups form the selective permeability barrier within the central pore. Figure created using BioRender.

2.1.2 Nucleocytoplasmic transport

Molecular transport through the nuclear pore can occur through either facilitated or passive diffusion**.** The permeability barrier formed by the central FG-Nups allows ions and small molecules of approx. less than 30-50 kDa (equivalent ~5 – 9 nm[25,26]) to freely diffuse through the NPC, whereas larger molecules rely on facilitated, receptor-mediated transport[27–29]. To overcome this permeability barrier, larger molecules targeted for nuclear import and/or export interact with nuclear transport receptors (NTRs), which can further interact with the central FG-Nups. For NTRs to interact with their cargos, the cargos must display specific amino acid sequences on their surfaces, which act as localization signals. These short signaling peptides can be classified as nuclear localization signals (NLS) and nuclear export signals (NES)[6]. NLSs are often short sequences of positively charged lysines and arginines, whereas NESs are rich in hydrophobic amino acids[30]. These signals are recognized by NTRs, also known as karyopherins, which mediate the trafficking of proteins across the nuclear envelope. These receptors are subdivided depending on the directionality of the cargo transport, although some of them have bidirectional transport capabilities[2]. Importins bind their cargo proteins in the cytoplasm and transport them to the nucleus. In eucaryotic cells, this nuclear import is carried out by importin α and importin β. In contrast, the nuclear export is carried out by exportins, of which CRM1 (Chromosomal Maintenance 1; also known as XPO1) is the most important and the best characterized one[8].

Overall, selective transport through NPC is a highly organized, rapid, and efficient process[9]**.** In the case of nuclear import, importin α recognizes the NLS on the cargo protein, which is further recognized by the carrier protein importin β (Fig 2). This trimer is transported into nucleus through the central channel. Once translocated in the nucleus, this complex is dissociated in the nucleoplasm by the action of RanGTP and the transport receptors are diffused back to the cytoplasm[2,31]. Conversely, during nuclear export, RanGTP binds and forms a complex with exportin and the NES-containing protein to be transported out of the nucleus (Fig 2). Once transferred into the cytoplasm, RanGTP is hydrolyzed into RanGDP, dissociating the complex and releasing the transported protein[15,31]. Different forms of Ran are asymmetrically distributed in the cell; RanGTP being enriched in the nucleus and RanGDP in the cytoplasm. Importantly, this RanGTP/RanGDP gradient across the nuclear membrane is essential in maintaining directionality of nucleocytoplasmic transport[15,32]. Although the precise mechanism of protein translocation through the NPC is not clearly understood, most of it depends on moderate affinity between the NTR-cargo complex and several nucleoporins[31,32]. NTR-bound

cargo molecules form transient complexes capable of interacting with FG-Nups in the central channel allowing them to cross the NPC. Since the rate of transport is very high, these interactions have to be relatively weak and transient for the cargos to move rapidly across the nuclear pore[25].

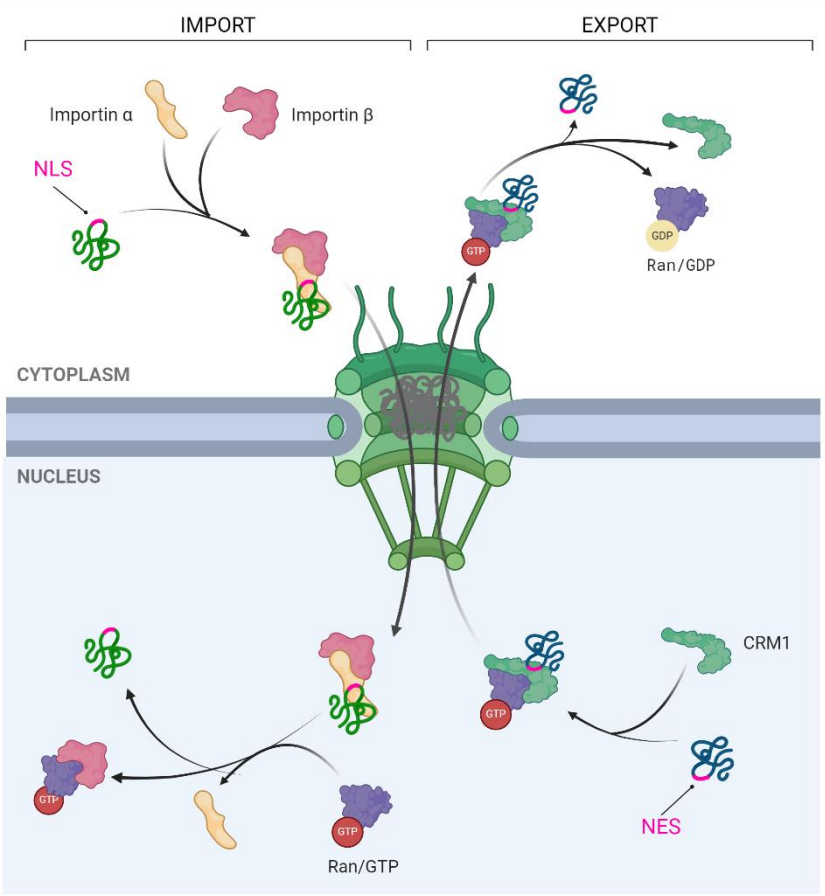

Figure 2 Schematic illustration of the facilitated nuclear transport through the nuclear pores. Left side shows the transport mechanisms in the case of import. In the cytoplasm, importin α binds to the nuclear localization signal within the cargo, which is then bound by the carrier protein importin β. This complex is shuttled across the nuclear pore by forming transient interactions with the FG-Nups. Within the nucleus, the complex in dissociated by the RanGTP and the cargo is released in the nucleus. Right side of the figure shows the transport mechanism in the case of export. In the nucleus, cargos containing a nuclear exit signal are recognized by exportins (CRM1), which form a complex with RanGTP. This complex is then translocated to the cytoplasm, where RanGTP is hydrolyzed into RanGDP, and the transported protein is released. Figure created using BioRender.

2.1.3 Regulation of nucleocytoplasmic transport

Several mechanisms are involved in regulating nucleocytoplasmic transport. As previously stated, the trafficking of larger molecules across the NPC is normally hindered,

unless they are bound to an NTR. Thus, export/import sequences must be accessible for the transporter receptors. Therefore, masking and unmasking of the localization signals within the cargo acts as a key mechanism for regulation of nucleocytoplasmic transport[5,33]. Another mechanism of regulation is post-translational modifications such as phosphorylation/dephosphorylation of sites near or within the localization signal[33]. Masking of the localization signal can also occur when localization signal-containing cargo proteins bind to specific cytoplasmic or nuclear factors, leading to the retention of the cargo in the cytoplasm or nucleus. One example of such is the glucocorticoid receptor (GR), which is retained in the cytoplasm through complexation with heat-shock protein HSP90. Upon ligand binding, GR is able to dissociate from HSP90 and translocate into the nucleus with the aid of NLS[34].

Nevertheless, not all protein trafficking of larger molecules is NTR-mediated. Although molecular size is the key determinant affecting the cargo transport, other factors can affect the transportation of large cargos and enable them to overcome the usual size limit of the NPC permeability barrier. For example, the shape[35] and mechanical stability[36] of cargoes, surface properties such as charge[37] and hydrophobicity[29] can all have an effect on the diffusivity through the NPC. In contrast, relatively small proteins that are highly charged, such as ribosomal proteins and histones, might require import receptors to pass through the NPC[37,38]. There is also growing evidence for alternative, non-canonical transport pathways. For example, proteins exhibiting structurally similar motifs of NTRs, such as beta-catenin, can bind directly to Nups[28,32]. Furthermore, and especially in the case of nuclear import, many proteins appear to utilize multiple nuclear transportation pathways. Exploiting multiple pathways for transport of the same cargo has been suggested to assure cellular functionality in the situations that one mechanism is inhibited or to adjust the nuclear transport based on cellular demand[39].

There is also increasing evidence that the size of the nuclear pore could influence the dynamics of protein transport. NPCs' pore size has been shown to change in response to environmental changes and mechanical stress. For example, in a study carried out by Elosegui-Artola et al. (2017), force applied to the nucleus using atomic force microscopy resulted in flattening of the nucleus and dilation of the nuclear pores. The apparent size of nuclear pores was also larger on cells seeded on stiff substrates. Also, active nuclear import was increased in both situations and in the case of force application, the transport was returned to initial values upon force release. Similarly, nuclear pores have been shown to constrict in different physiological conditions such as under conditions of cellular energy depletion and hyperosmotic shock[14]. Under both conditions, passive nuclear

import was reduced. These studies have suggested, that dilation and restriction of the nuclear pores is caused by increased or reduced nuclear envelope tension, respectively[14,40].

2.2 Cellular responses to external mechanical stimuli

Cells are constantly sending and receiving both chemical and mechanical signals from the extracellular matrix (ECM) and neighboring cells. In addition to biochemical cues such as cytokines and growth factors, cells are subjected to complex tensile and compressive forces as well as shear stress[41,42]. In order to maintain homeostasis, cells must be able to sense and respond to these mechanical cues from their microenvironment - a process also known as mechanosensing[41]. Physical cues are then transferred and transformed into a biological response, which is a process known as mechanotransduction[43,44]. Although cells can adapt to their microenvironment and fine-tune their mechanical properties to match the forces they encounter, drastic alterations in cells microenvironment, such as strong forces may cause alterations in cell's regulatory mechanisms[44,45].

Mechanical signaling has the potential to transmit information very quickly. For any distance greater than tens of nanometers, mechanical signal can arrive in microseconds compared to seconds or minutes for diffusion[43,46]. Application of mechanical stimulus can activate multiple complexes at the plasma membrane such as stretch-activated ion channels, cadherin assemblies at cell-cell junctions and other signal-transducing proteins [47,48]. Ultimately these external forces activate a variety of signaling pathways and genetic programs to regulate cell behavior[45].

Mechanosensing and -transduction play a direct role in various cellular processes such as stem cell differentiation, cellular motility and proliferation[47,49,50]. Mechanosensing also plays a fundamental role during various stages of embryonic development[45]. It is therefore not surprising that defects in cellular mechanotransduction have been associated with several diseases including fibrosis, atherosclerosis, compromised immune response as well as tumorigenesis and metastatic progression[51–53]. Although not exclusive, disruption in force transmission between the ECM, the cytoskeleton and the nucleus, is a common factor related with such mechanotransduction-related diseases.

In the following chapters, cellular mechanosensing and -transduction will be further introduced, focusing mainly on the mechanical cues arising from the cell-ECM interface,

and how these signals are transmitted via the cytoskeleton to the nucleus. In addition, the role of the nucleus as a mechanosensor will be discussed in more detail.

2.2.1 Mechanosensing at adhesion sites

Cells in tissues are constantly probing the surrounding ECM through a number of cell surface proteins, of which the most fundamental ones are integrins[54]. During migration, cells must detect the physical properties of the EMC and in response, apply the right forces to move. Such adhesion of cells to the ECM mainly relies on integrins, which are the major adhesion receptors for EMC proteins. Integrins cross the plasma membrane and form the main mechanical link between the ECM and the cellular cytoskeleton[55] (Fig 3a). Integrins are composed of α and β subunits which each recognize specific ligands of ECM[56]. Integrins can be activated from both inside and outside of the cell, and this bidirectionality allows cells to sense and adapt to the ECM properties to control migration, proliferation and differentiation[57,58]. Integrins are the most abundant proteins at focal adhesions (FA), which are among the most studied mechanosensory complexes located at the cell membrane-ECM interface[47,48]. FAs are highly dynamic complexes, and their formation and maturation is dependent on the presence of force[44,57,59]. Cells usually generate higher traction forces on stiffer substrates, thus FAs are more abundant and matured when cells are cultured on a stiff surface, e.g. when cultured on glass or plastic[47,60].

In addition to mechanotransduction occurring at the cell-ECM interface, cells also exert mechanical forces on one another at cell-cell adhesion sites. Adherens junctions (AJs) are the primary structures for cell–cell adhesion, playing a crucial role in maintaining the mechanical integrity of tissues. AJs are generally composed of cadherins, which are transmembrane proteins that interact with identical molecules on adjacent cells[61,62]. Intracellularly, cadherins bind to catenins (p120 catenin, α-catenin and β-catenin) which can activate various signaling pathways to regulate cytoskeleton reorganization, differentiation, and the cell cycle[61,62]. Cadherin-associated cytoplasmic partners also connect directly or indirectly to actin via vinculin[61,63]. Thereby, they link cell–cell interactions to the actin cytoskeleton. Furthermore, AJs interact with FAs, both functionally and structurally, through the cytoskeleton allowing crosstalk between these adhesion complexes. In all, this enables cells to integrate mechanical signals from both their surroundings (ECM) and neighboring cells, contributing to processes like migration, polarity, and tissue integrity[61,63].

2.2.2 Force propagation through the cytoskeleton to the nucleus

Upon mechanical stimuli, the outside-in activation of integrins by conformational changes leads to signal propagation to the cytoskeleton, mostly the actin cytoskeleton[57]. As the cytoplasmic domain of integrin lacks an actin binding site, other submembrane proteins at FAs are required to complete the actin–integrin–ECM linkage[64]. Of these intermediate proteins especially talin and vinculin are considered as fundamental mechanosensors[59,65,66]. Upon the application of force, these focal adhesion proteins undergo conformational changes which can both reinforce protein-protein interactions and reveal binding sites upon protein unfolding[48]. Especially the binding of talin to integrin β subunit is shown to be crucial in integrin activation[67]. This activation initiates signaling cascades that ultimately lead to cytoskeletal rearrangements and reinforcement through actin polymerization and actomyosin contractility[57] (Fig 3b).The cell's actomyosin network undergo continuous assembly and disassembly allowing cells to maintain cellular tension and undergo modification when sensing substrate rigidity and mechanical stress[68].

It is widely known, that tension force results in formation of contractile actomyosin bundles called stress fibers (SF)[60,69]. In most cases, SFs are connected to focal adhesions [70]. One subtype of SFs is the perinuclear actin cap. The actin cap is composed of thick and highly contractile bundles of actomyosin filaments wrapped over the nucleus[71,72]. The actin cap plays an important role in maintaining and regulating the nuclear shape and position[73,74]. It is also shown to protect the nucleus from mechanical damage[75].

The actin fibers and in particularly the actin cap ultimately transfer the external mechanical stimuli to the nucleus. The actin cap is tightly attached to the apical surface of the nucleus through the Linker of nucleoskeleton and cytoskeleton (LINC) complex[60,71] Therefore, the cytoskeleton and the interior of the nucleus are mechanically coupled through the LINC complex[76,77](Fig 3c). LINC complexes are composed of KASH (Klarsicht, ANC-1, and Syne Homology) and SUN (Sad1, UNC-84) proteins which are localized at outer (ONM) and inner nuclear membrane (INM), respectively[77]. SUN proteins are organized in trimers residing at the INM which bind three KASH proteins in the perinuclear space[77]. SUN proteins extend into the nucleoplasm and form connections with the nuclear lamina and chromatin[71,78]. SUN proteins are also known to interact with the nuclear basket protein Nup153[26,79]. KASH proteins are tail-anchored in the ONM which interact with the cytoskeleton directly or through linker proteins[77].

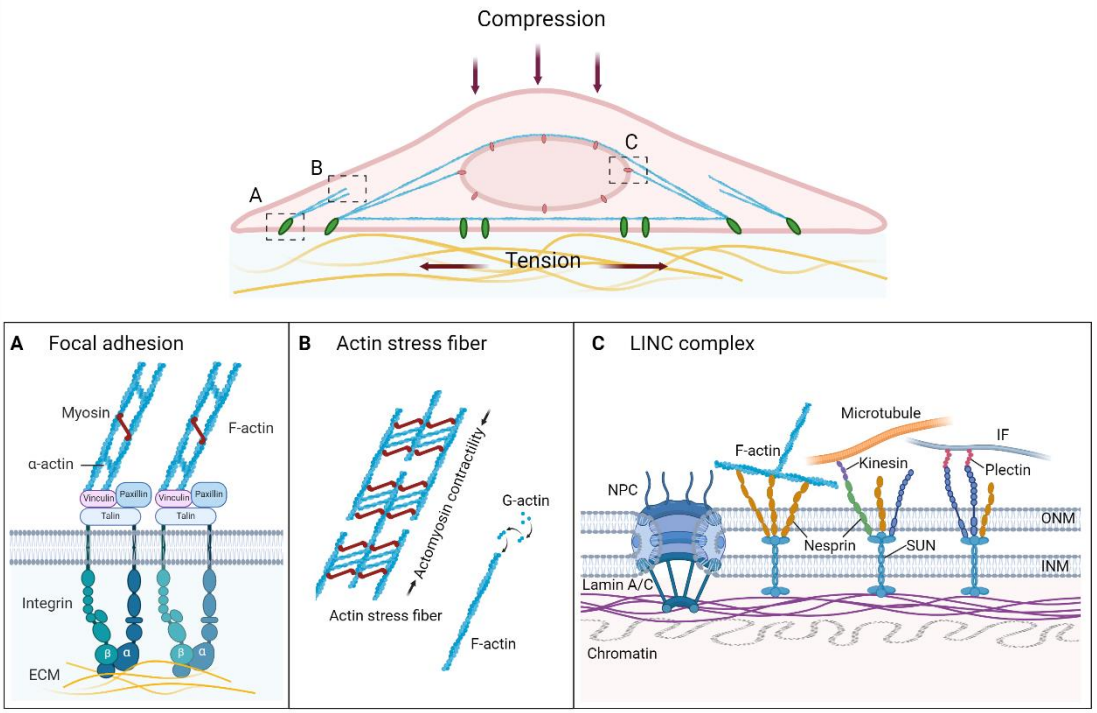

Figure 3 Schematic illustration of main features governing the mechanotransduction from the ECM to the nucleus. A) At focal adhesions, integrins form connections with the ECM proteins as well as with submembrane proteins such as talin, vinculin, paxillin, which ultimately connect integrins to the actin cytoskeleton. Upon force application, these proteins undergo conformational changes which can both reinforce protein-protein interactions and reveal binding sites upon protein unfolding. B) Integrin activation ultimately leads to cytoskeletal rearrangements and reinforcement through actin polymerization and actomyosin contractility. Tension force usually results in formation of stress fibers. C) On the nuclear envelope, actin stress fibers are connected to the nucleus via the LINC complex, which forms a direct mechanical link between the cytoplasm and the nucleus. In the cytoplasm, nesprins interact either directly or indirectly with the cytoskeleton, whereas in the nucleoplasm, SUN proteins are known to interact with the lamina and chromatin. Figure created using BioRender.

2.2.3 Nucleus as a mechanosensor

Whereas mechanosensing at the plasma membrane has been shown to play a central role in mechanotransduction, it now emerges that the nucleus itself may act as a mechanosensitive structure. The nucleus is the largest and stiffest cellular organelle, which can dynamically alter its morphology and mechanical properties, enabling it to adapt and function in various mechanical environments[74,80]. For example, while stem cells modify their nuclear envelope and chromatin structure during differentiation that leads to nuclear stiffening, segmented nucleus of a neutrophil enhances nuclear plasticity, easing the migration of the cells through confined spaces[80].

Underneath the inner membrane of nuclear envelope lies the nuclear lamina, which is a dense 10-30 nm-thick complex network of type A- and B lamins, and lamin-binding proteins[80,81]. In mammalian cells, the type A lamins include lamin A and C which are two splice isoforms encoded by LMNA gene[80]. The nuclear lamina governs many critical functions from regulating chromatin organization and transcription to providing structural support. Specifically, lamin A is known to have a crucial role in determining nuclear shape and stiffness[74]. Consequently, mutations and altered expressions in lamin A/C have been shown to correlate e.g. with defects in nuclear stability and nucleo-cytoskeletal force transmission[81]. The lamina also interacts with heterochromatin in lamin-associated domains (LADs)[82]. Lamins are also connected to a variety of nuclear proteins, including the NPCs on the nuclear membrane, where they have been shown to regulate their distribution[83]. Direct force application to the nucleus has also been shown to induce chromatin stretching[81].

As previously mentioned, the nuclear lamina also has a direct connect to the cytoskeleton through the LINC complex. In a study performed on isolated nuclei, Guilluy et al. (2014) showed that the nucleus can adjust its stiffness in response to force application. This adjustment was done through recruitment of lamin A/C to the LINC complex when force was applied to KASH proteins[84]. It is largely accepted, that for cells to effectively transmit forces between the nucleus and the cytoplasm, an intact LINC complex is required. For example, the loss of LINC complex and thus impaired nucleo-cytoskeletal coupling is linked to muscular dystrophies and reduced migration capabilities of endothelial cells[81].

There has been much discussion about the possible mechanics how a mechanical stimulus might affect the confirmation and function of the NPC. As previously stated, it is suggested that there is a connection between the mechanical status of the NE/membrane tension and NPC diameter. When cells are cultured on rigid or stiff substrates, focal adhesions and stress fibers are formed leading to nuclear flattening. This then stretches and curves the nuclear pores[40] possibly due to increased tension across the nuclear envelope. Similarly, decrease in NPC diameter has been reported in hyperosmotically shocked cells[14]. Also, possible reassembly of the FG-Nups upon mechanical stimulus might reduce its mechanical resistance[40] thus affecting the permeability barrier of the NPC. Additionally, changes in the conformation of the nuclear basket could potentially alter the flux for the transported proteins.

Since the NPC has been shown to be mechanosensitive, it is reasonable to think about its effects on protein transportation across its interior upon mechanical stimuli. According to the study of Elosegui-Artola et al (2017), the nuclear flattening and thus stretching of the nuclear pores lead to increased import of a mechanosensitive transcription factor YAP to the nucleus in epithelial cells. In another recent study by Ghagre et al (2024) they showed higher passive nuclear import of YAP via NPC with increasing nuclear curvature in mesenchymal stem cells[85]. Overall, the size alteration of the nuclear pores could strongly affect the import and export of both actively and passively transported proteins, such as transcription factors, which ultimately could alter the gene expression. However, the precise impact of NPC constriction or dilation on the passive and active transport of various types of cargo is yet to be fully understood.

Although external forces may not directly reposition chromatin or modify gene expression, they can trigger a remodeling process at the NE, which plays a crucial role in downstream signaling cascades. For example, nuclear loading may result in remodeling of the nuclear lamina, which then changes the binding properties of NE proteins and transcription factors[86]. Such example is emerin, which in shown to affect mechanosensitive gene expression[87].

In all, the nucleus responds to mechanical stimuli through various mechanisms, many of which remain unclear and underexplored. It is now well recognized that the nucleus and nuclear proteins play a vital role in the cellular response to mechanical stimuli, and that forces are transmitted from the cell surface and cytoskeleton to the nuclear interior. However, distinguishing the effects of direct force applied to the nucleus from those that arise secondary to changes in cytoplasmic mechanosensitive signaling pathways is challenging. It is also worth noting, that the cell's response to mechanical stimuli is ultimately regulated by a complex interaction of mechanical and biochemical feedback loops working in coordination.

2.3 Optogenetics

Optogenetics is a technique that uses a combination of light and genetic engineering to control the activity of a cell. This is achieved by introducing foreign genes into the target cells leading to the expression of light-sensible proteins[4]. The term was first coined among neuroscience in 2006 by Karl Deisseroth et al, following their studies in using microbial channelrhodopsin-2 (ChR2) to stimulate mammalian neurons with light[88]. Optogenetic tools are engineered to perform a certain biological function only after absorption

of light of a specific wavelength enabling modulation of protein functions *in vivo and in vitro*. By using lasers, light can be applied with very tight spatial resolution, and it can be rapidly turned on and off. These tools can provide temporal resolution of milliseconds to seconds allowing for specified cellular manipulation[88]. Optogenetic tools can also provide quantitative methods to assess various dynamic cellular processes. Importantly, off-target effects and cytotoxicity are often reduced with optogenetic tools, whereas chemical inducers often suffer from promiscuous binding profiles[30,89,90].

Optical stimulation has been utilized in both *in vitro* and *in vivo* studies, for example in the case of neuron firing[91] and heart beating[92]. While optogenetics have a long history in neuroscience in controlling neuronal activity through light-sensing channels and pumps, more recently a variety of optogenetic tools have been expanding to broader fields of cellular biology and biotechnology. Among the field of cell biology, optogenetic tools have been developed and utilized in controlling and manipulation of a wide range of cellular functions such as membrane localization[93], protein concentrations[94], nucleocytoplasmic transport[5,95–98] as well as in gene editing[99].

Each optogenetic protein contains a light-responsible domain that is coupled to a biological function. In nature, a wide variety of photoreceptor proteins have evolved, each with distinct biochemical and physical properties. These photoreceptor proteins contain chromophores which have the intrinsic capacity to absorb light leading to conformational changes within the protein[100]. Several of such photo-sensitive proteins have been used as tools for the generation of optogenetic systems. One widely utilized photosensitive domain is the light, oxygen and voltage (LOV) domain isolated from plant photosensor phototropin1[101]. This domain provides the ability to control the protein's active and inactive states through photocaging[101]. A conformational change triggered by light enables the protein to interact with its substrate or target protein. Such LOV-based optogenetic tools have been shown to be effective in regulating protein levels within specific subcellular compartments, including the nucleus[30,100].

Screening the optimal experimental conditions is important when setting up experiments using optogenetics. Despite the advantage of low toxicity with light activation, illuminating cells using fluorescence microscopy causes inevitable phototoxicity and photobleaching[102]. In order to minimize these and other possible side effects, optimization of the illumination input, i.e. timing, duration, location, and intensity is crucial[101]. Ideally an optogenetic tool works at low illumination intensities, having great sensitivity and specificity

to low levels of activation light. Other important characteristics of an optogenetic tool include the dynamic range, dark state leakage, reversibility, and photostability[103].

2.3.1 Light-inducible nuclear export system (LEXY)

For precise and specialized cellular functions, most cellular processes must take place at specific times and locations within the cell. Therefore, the activation of the appropriate proteins must happen at the right place and time. Proteins can be either maintained in their correct locations and be inactive until needed, or they can alternatively be transported to the correct location when needed. One notable example of the latter is the translocation of transcription factors from cytoplasm to the nucleus and further binding to appropriate DNA sites[30]. Since many signaling events eventually lead to changes in gene expression, several optogenetic tools have been developed to allow the studying and manipulation of such nucleocytoplasmic protein transport.

One such example is the Light-inducible nuclear export system (LEXY) developed by Dominik Niopek et al (2016)[5]. LEXY exports tagged proteins from the nucleus to the cytoplasm under the illumination of blue light (440-473 nm)[103]. The system is based on *Avena sativa* (oat) LOV2 domain (AsLOV2), a small protein, with a C-terminal Jα helix that unfolds in response to blue light. The LOV2 was engineered to contain a strong nuclear export signal (NES) photocaged within the Jα helix. Upon blue light illumination, the unfolding of the α helix results in exposure of the NES. The NES is then recognized by the exportins and upon binding, the construct is exported from the nucleus to the cytosol. The construct also has a weaker NLS which localizes the construct in the nucleus in the dark state. The system is fully reversible, and the nuclear localization is recovered in the dark within about 15 minutes.

LEXY has been reported to work on multiple cell types from mouse to human[104]. In theory, any protein of interest (POI) can be fused to the LEXY construct, and it has been successfully used for example in controlling transcription of specific genes with tagged receptor proteins. Owing to its high spatiotemporal control, LEXY-tagged tumor suppressor p53 have shown promising results in regulating cellular p53 levels. Niopek's team also tagged LEXY with the chromatin-anchored histone H2B which resulted in light-dependent sequestration of endogenous CRM1 receptors thus blocking the export of other cargo[5].

LEXY was used in this work to study nucleocytoplasmic transport in epithelial cells. The specific LEXY construct used in this work contains an mCherry fluorescent protein which provides a fluorescent readout for the location of the construct. An illustrative image of the construct in shown in Figure 4. Hereafter, this NLS-mCherry-AsLOV2-NES -construct will be called solely as “LEXY”. This tool was optimized for Tampere University imaging set-up using confocal microscopes and it was further employed in semi-quantitative studies of nucleo-cytoplasmic transport in live cells encountering mechanical perturbations.

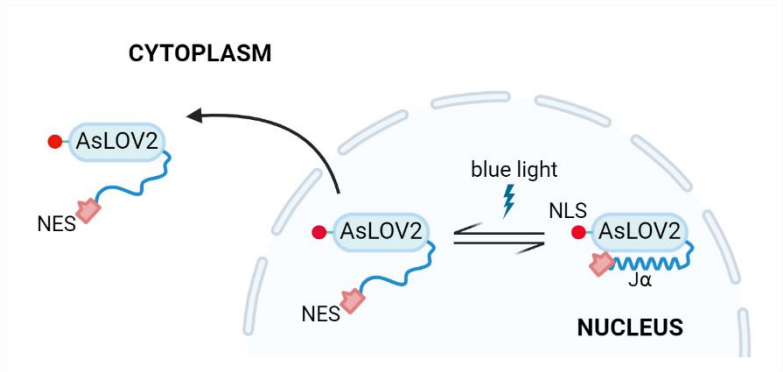

Figure 4 Schematic of LEXY function. Blue-light irradiation leads to exposure of the photocaged NES signal in the AsLOV2 domain, resulting in nuclear export of the construct. A weaker NLS fused to mCherry is always active and in the dark state, the construct is recovered and shuttled back to the nucleus within 15 min. Figure created using BioRender.

3. AIMS OF THE STUDY

The broader aim of the thesis is to study the variations in nucleo-cytoplasmic transport during changes in mechanical properties of the nucleus.

Specific Aims:

1. Optimize the LEXY imaging and light stimulation parameters
2. Construct epithelial cell lines (MCF-7 And MDCK) stably expressing LEXY-system
3. Study nucleo-cytoplasmic transport rates during mechanical manipulation of cells

4. MATERIALS AND METHODS

4.1 Cell lines

Madin-Darby canine kidney II (MDCK II) and Michigan Cancer Foundation-7 (MCF-7) cell lines were used to construct cell lines expressing LEXY. Both cells were grown in Minimum Essential Media (MEM) with GlutaMAX™ (Gibco, Thermo Fisher Scientific, 41090-028) supplemented with 10 % fetal bovine serum (Gibco, 10500064) and 1 % penicillin-streptomycin (Gibco, 15140122). For MCF-7 cells, the media was also supplemented with 1 % MEM Non-Essential Amino Acids (100X) (Gibco, 11140-035) and 0.01 mg/ml insulin (Sigma-Aldrich, I9278). Cells were cultivated at 37 °C and 5 % CO_2. Media was changed every 2-3 days and cells were passaged every two weeks (MCF-7) or once a week (MDCK II). In the generation of stable cell lines, after selection with geneticin the G418 concentrations were kept at 250 µg/ml during cultivation. After transfections cells were cultured in dark conditions to avoid premature activation.

4.2 Transient transfection with Fugene HD

MDCK II and MCF7 cells were seeded on collagen I-coated 22 x 22 coverslips in a 6 well-plate. After 24 hours at around 50 % confluence, each well was transfected with 2 µg of LEXY-plasmid using Fugene HD (Promega). For four reactions, a Fugene Master Mix was prepared with 27 µl of Fugene and 360 µl of clean MEM (no additives). The solution was left to incubate for 5 min at RT. Per each reaction, 2 µg of DNA was first mixed with 20 µl of clean MEM and mixed with 80 µl of the diluted Fugene solution. The solutions were left to incubate for 10 min at RT and transfection mixtures were transferred to 6-well plate wells having 2 ml of complete MEM. Cells were incubated for 3 days before imaging.

4.3 Stable cell line generation

4.3.1 Transfection with Neon electroporation system

Stable MDCK II and MCF-7 LEXY cell lines were generated by using Neon Electroporation System (Thermo Fisher Scientific, MPK5000). Cells were washed twice with phosphate buffered saline (PBS) and trypsinized with 0.25% Trypsin-EDTA (Gibco, 25200- 056). For MCF-7 cells the incubation time was 5 min and for MDCK II cells 15

min at 37 °C. For each transfection, 1.2 x 10^6 cells were counted using a Bürker chamber and cells were pelleted (1000 rpm, 5 min, room temperature). Cells were resuspended in Buffer R (Invitrogen, Neon Transfection System Kit, MPK10096). The NLS-mCherry-LEXY (pDN122) plasmid was provided by the thesis work instructor and the information is provided in Figure 5. For each transfection, 2.5 µg of the plasmid was used, and electroporation was performed using different programs for both cell lines. A single pulse of 1650 V voltage and 25 ms was used for MDCK II cells and two pulses of 1100 V voltage and 30 ms were used with MCF-7 cells. Transfected cells were transferred to fresh MEM and plated in culture vessels. After 24 hours of incubation at 37 °C, the media was supplemented with a selective antibiotic G418 (Roche) at concentrations of 400 µg/ml (MCF-7) and 750 µg/ml (MDCK II). With MDCK II cells, the concentration of G418 was lowered to 500 µg/ml after a few days. Cells were cultured in these conditions for 2.5 weeks until FACS sorting.

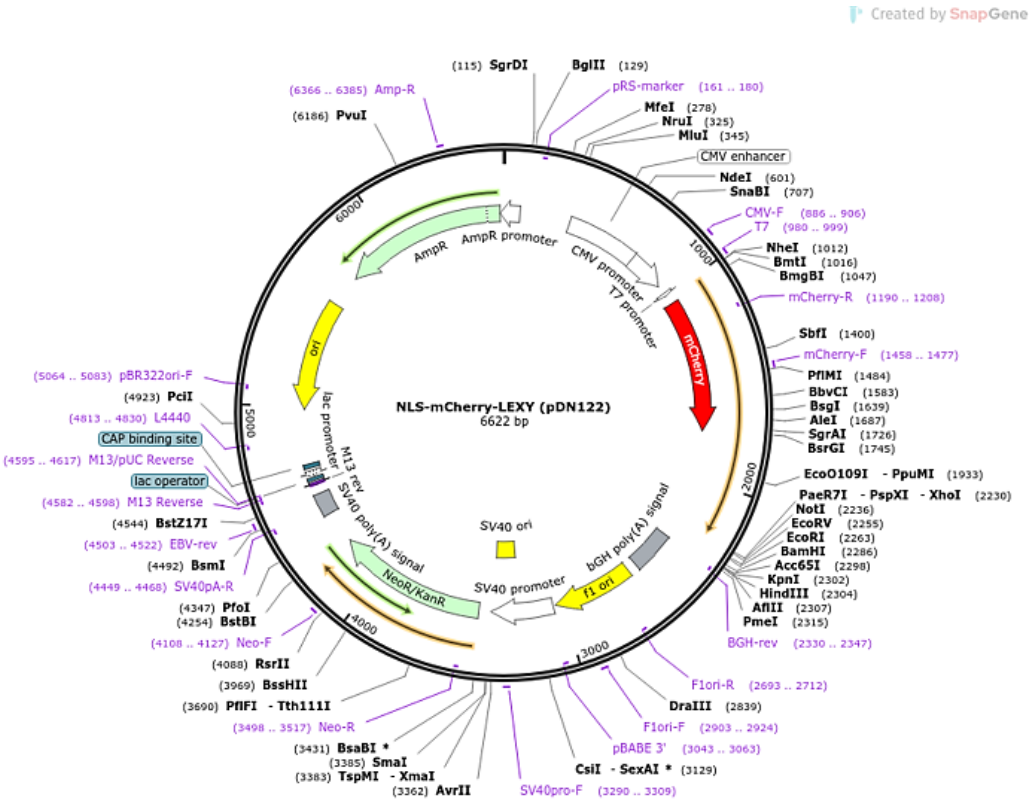

Figure 5 LEXY plasmid. Image from: https://www.addgene.org/72655/

4.3.2 Fluorescence-activated cell soring (FACS)

Transfected MCDK II-LEXY and MCF-7-LEXY cells were observed under confocal microscopy (Zeiss LSM 780) to verify the LEXY expression. Both cell lines were FACS

sorted (BD Biosciences, BD FACSAria™ Fusion Flow Cytometer) in the university FACS core to sort cells expressing mCherry fluorescent protein. Cells were sorted on plates with HEPES media (10 mM HEPES in MEM) and after 48 hours media was changed to complete MEM and G418 was added at selection concentrations. After 3.5 weeks, both cell lines were FACS sorted once more, and all but single-cell activation tests were conducted with these cells in this work.

4.4 Cytoskeletal disruption by cytochalasin D and nocodazole

For degradation of the actin cytoskeleton and disruption of microtubule function, cells were treated with 10 µg/ml cytochalasin D (Sigma Aldrich) and 20 µM nocodazole (Carbosynth). Cells were incubated in drugs-supplemented media for 30 min prior fixation or live-cel imaging.

4.5 Polyacrylamide gel cushions

4.5.1 Coverslip cleaning and activation

Bottom (d13mm, VWR) and top (18 x 18 mm, Carl Zeiss) coverslips were cleaned in 2% Hellmanex solution (Sigma Aldrich) in an ultrasonic bath for 30 min at RT. Cleaned coverslips were washed with excess dH_2O and immersed in dH_2O and 99 % EtOH. Coverslips were dried with N_2 stream in the laminar hood. Bind-silane was used to make the PAA gel cushions to stick to bottom coverslips. Bind silane-solution was composed of 94,7 % ethanol (95 %), 5 % acetic acid (Galacia) and 0.3 % bind-silane (Sigma, 3-(Trimethoxysilyl)propyl methacrylate). 10 µl of the solution was pipetted on each bottom coverslip and after 3 min of incubation, the coverslips were washed with ethanol and dried with N_2 stream.

4.5.2 Polyacrylamide gel preparation

Acrylamide solution (Bio-Rad) bis-acrylamide solution (Bio-Rad), 10X PBS and ddH2O were mixed for respective contents of 5 %, 0.15 %, 10 % and 84.85 % to obtain a gel of 4.5 kPa Young's modulus. The solution was degassed in a vacuum chamber to remove the oxygen dissolved in the solution which would inhibit the polymerization. After degassing, the solution was mixed with 0.2 % TEMED (Bio-Rad) and 0.1 % ammonium persulfate (Sigma Aldrich, first diluted in 10 % w/v ddH2O). The solution was mixed by inverting the tube 5 times and casted on bind-silane activated coverslips in Eppendorf lids. The gel drops were covered with 2 % HellmaneX-cleaned 18 x 18 mm coverslips and let

polymerize for 15 min. After polymerization, the lids were inverted, gel cushions were detached from the lids and spacers were glued on top of the gels for extra weight. Gels were stored in 1X PBS at + 4 °C.

4.6 Immunostaining

Cells were seeded to collagen I (Gibco, A1048301) coated high-precision 22 x 22 mm coverslips (0.17 mm) and grown for 4 days until reaching 80 % confluency. Coverslips were rinsed with 70 % and 100 % ethanol and dried in laminar flow hood. Coverslips were incubated with 500 µl collagen I solution (150 µl/ml, in 0.02 N acetic acid) for 1 hour of which first 20 min under UV light. Coverslips were washed twice with 1X PBS, provided with fresh media and incubated for 25 min at 37 °C and 5 % CO_2 before seeding the cells.

Cells were fixed with 4 % paraformaldehyde (Gibco, 14190-094) for 15 min at RT in dark, and washed twice with 1X PBS. Cells were permeabilized with 0.5 % BSA (PAN-Biotech) and 0.5 % Triton X-100 (Sigma Aldrich) in 1X Dulbecco's Phosphate Buffered Saline (DPBS, Gibco) for 10 min at RT. Some samples were stained for nuclear pore complex proteins; primary antibody (Abcam, mouse monoclonal ab24609, 1:500) and secondary antibody Alexa Fluor 647 (Thermo Fisher Scientific, 1:1000). Both antibodies were diluted in 3 % BSA-PBS. Samples were incubated with the primary antibody for 1 hour at RT in dark and washed three times with permeabilization buffer, 1X PBS and permeabilization buffer for 10 min each. Samples were incubated with the secondary antibody for 1 h at RT in dark and washed twice with 1X PBS for 10 min. Some samples were stained with phalloidin (ATTO-TEC, ATTO 643, 1:60) for F-actin and counterstained with DAPI (1 mg/ml, 1:1000). Both phalloidin and DAPI were diluted in 1X PBS. Samples were incubated with phalloidin for 1 h at RT and washed twice with 1X PBS for 10 min. Staining time for DAPI was 5 min at RT followed by a 10 min 1X PBS wash and a 10 min dH_2O wash. Samples were stored in 1X PBS at + 4 °C in dark until imaging.

4.6.1 Microscopy

Confocal images of fixed cells were taken with Zeiss 780 with Apo 63x/1.40 Oil DIC objective. Nuclear pores were imaged using 633 nm for excitation and 677/35 nm for emission. mCherry was imaged with 561 nm excitation and 601/62 nm emission. For DAPI and F-actin, the excitation lasers and emission filters were ex:405 / em:498/175 (DAPI) and ex:633 / em:699/121(F-actin).

4.7 Live-cell imaging

Before imaging, all samples were incubated and transported protected from light to avoid premature activation due to white light exposure.

4.7.1 Single-cell activations

Images were acquired with confocal microscopes system equipped with automated temperature (37 °C) and CO2 (5%) controls. Activation of the LEXY-construct in MDCK II single cells was performed using Zeiss LSM 780 with a 63x / 1.40 Oil DIC a Plan-Apochromat objective. A rectangular region of interest (ROI; 3 µm x 3 µm = 9 μm^2) was selected and placed onto single selected cells. The ROI was scanned with a 458 laser for 20 sec at 50 % laser power following a 10-min dark-recovery phase. The activation was repeated after 10 min. mCherry was imaged in parallel every 20 sec with a 561 nm laser (0.3 % power, 875 gain). For the 552 x 552 image the pixel size was 0.098 µm, zoom was 2.5, and the pinhole was 61.1 µm. Frame time was 2.09 s.

4.7.2 Whole-field-of-view activations

Activations were done by selecting the whole field of view as the ROI. These activations were done for both cell lines for the control samples and in different experimental settings: after cytoskeletal disruption with cytochalasin D, and with weights being placed on top of the cells. Two rounds of stimulations followed by a recovery phase were done for the same cells. First round acted as a control and before starting the second round, cells were either treated with cytochalasin D and nocodazole or weights were placed on top of the cells. Since not a 100 % of the cells were expressing the LEXY construct, a spot having approximately a few tens of expressing cells were located with the microscope, ideally having similar steady-state mCherry intensities.

MDCKI II-LEXY cell images were obtained using Zeiss LSM 780 with a 63x / 1.40 Oil DIC Plan-Apochromat objective. A baseline of mCherry fluorescence was first captured with the 561 nm laser (10 images). Photoactivation was done with the 488 nm laser by using 5 iterations of a 1.92-sec pulse (100 % laser power) following an mCherry image being captured with the 561 nm laser (0.15 % power, 825 gain). The pixel size and zoom for 1024 x 1024 images were 0.219 µm and 0.6 for all MDCK-LEXY images, except for the MDCK-LEXY sample with heavier weight, where for 512 x 512 images the zoom was 1.2. In this case, the 561 nm laser power was 0.3 % and gain was 825. Frame time was

1.92 s for all but the MDCK-LEXY sample with heavier weight, where frame time was 0.782 s. Total blue light illumination time was approximately 5 - 6.7 min. In all cases, the recoveries were followed by capturing an mCherry image every 90 sec for 25 min to 1 hour. These steps were then repeated for the same sample.

For the MCF7-LEXY cells, images were acquired with Nikon A1R with a 40x / 1.15 LWD water immersion λS objective. After capturing the baseline of mCherry, photoactivation was done with the 488 nm laser (10 % power with ND filter) for a total 3.3 min, of which the blue light illumination time was approximately 1.3 min. An mCherry image was captured in parallel with the 561 nm laser (10 % power with ND, 200 gain) after each stimulation. With all samples and 1024 x 1024 images the pixel size and zoom were 0.12 µm and 2.7. Frame time was 2.11 s. The recovery of the construct was followed for 25 – 40 min by capturing an mCherry image every 1 min.

4.8 Image analysis

All microscopy images were analyzed using ImageJ (version 1.53t). Each cell was analyzed separately from the original image stacks. First, the time lapse videos were aligned using the plug-in StackReg to correct any possible sample drift. Z-projects with average intensities were taken from each stack for localization of the nucleus. A perinuclear ring was drawn manually on the outer boarder of the nucleus (width 0,8-1,2 µm) and this ROI was used for measuring the mean intensity values of the cell cytoplasm. Nuclear intensities were calculated using mean intensity values of circular ROIs (5 – 8 μm^2). Using these ROIs, measurements were conducted in whole stack. Background intensities were calculated from a region far from the cells. All data was then collected into and analyzed in Microsoft Excel (version 2303).

Background intensities were first subtracted from both nuclear and perinuclear intensity values. Nuclear and perinuclear intensity ratios (N/C) were then calculated by dividing nuclear intensities by cytoplasmic intensities. For visualization purposes, the data was normalized to the averaged N/C_0 value before first photoactivation. For both cell lines, the measurements were conducted to n=5 in each experimental setting, except in the case of MCF7 control, where n=3.

4.8.1 Curve fitting

Import rate constants of the LEXY construct were estimated in all experimental settings based on the first 25 (MDCK II) or 38 min (MCF7) recovery datapoints after both rounds of photoactivations. Normalized and background-corrected nuclear to cytoplasmic intensity values were fitted to an exponential equation: $I_{N/C}(t) = I_{N/C}max * (1-e^{-kt})$, where $I_{N/C}max$ = fluorescence intensity at steady-state and t = time. From this equation, the rate constants (k) were derived.

4.8.2 Statistical analysis

For the kinetic analysis, curve fitting was performed on individual cells for both recoveries. Shapiro-Wilk normality test was used to verify that samples were normally distributed and paired t-test was used to find significance within groups. P-values ≥ 0.05 were considered statistically not significant.

5. RESULTS

5.1 Setting up the LEXY system

Testing of the LEXY construct started with transiently transfected MDCK II cells. The optimal light-dose required to fully activate the system without causing detectable phototoxicity was determined experimentally by changing the light stimulation parameters, such as the stimulation wavelength, frequency, exposure time and intensity. The light dose was determined to be optimal once the nuclear mCherry had reached a plateau phase (minimal intensity) following a continuous increase in the dark state. Too short stimulation times had no or little effect on the construct, whereas high intensities and long stimulation times resulted in high phototoxicity and/or bleaching leading even to cell death and minimal if any recovery during the dark state.

In single-cells, a good response was achieved using the following parameters: a ROI of 9 µm2 was placed in the nucleus and stimulated with 0.36-sec 458-nm laser pulses for 18 sec (50 iterations) at 50 % laser power of LSM 780 confocal system. After the stimulation, ~ 90 % recovery of the initial nuclear mCherry fluorescence was observed within about 10 min. After the recovery, stimulation could be repeated 2-3 times without affecting cell behavior or showing visible adverse effects during imaging. Each time this resulted in over 30 % decrease in nuclear mCherry intensity within 1 min from start of the stimulation (Fig 6).

Since the activation of the construct happened very fast within single cells, we decided to test the response of the construct over a longer period with a larger ROI. Eventually, the construct seemed to work with stably transfected MDCK II cells when the whole field of view was selected as a ROI. This enabled several cells to be studied simultaneously. The parameters for the whole-field-of-view stimulations were quite different compared to those of single cells; the stimulation was done with the 488 nm laser at 100 % laser power. The total time of stimulation followed by an image capture was 8.5 min of which blue light exposure was approximately 5 - 6.7 min (1.92-sec pulses, 5 iterations, 30-40 cycles).

Photobleaching was an inevitable problem with such long time-lapse imaging of the whole field of view, especially during the stimulation phase. The bleaching effect could

be seen as a decline in cytoplasmic mCherry intensity. This could be somewhat decreased by lowering the 561 nm laser power from 0.2 % to 0.15 % and increasing the detector sensitivity (PMT gain), which resulted in less bleaching of the sample without adding too much background/noise to the image. After the first photoactivation, the nuclear mCherry intensity dropped to ~10 % and the cytoplasmic intensity dropped to ~30 % of the initial intensity values. After the second stimulation, the corresponding values were ~10 % and ~60 % (Fig 7c).

Another problem with the long lasting live-cell imaging experiment is the change of focus due to cell and sample movement. This can be seen in small sudden changes in intensity values in Figure 6. For that reason, instead of following only the nuclear mCherry intensity, the change in intensity across time was visualized as nuclear to cytoplasmic ratio (N/C). This minimized the possible error in intensity values caused by cell movement. N/C values were normalized to the mean baseline value prior the first stimulation. After the stimulations, the N/C ratio values dropped to 21 ± 8 % and 17 ± 4 % of the baseline values. (Fig 7d)

During the 40-min recovery periods, the N/C ratios did not show full recoveries back to the baseline values. After the first photoactivation, the N/C ratio was 88 ± 3 % and 89 ±

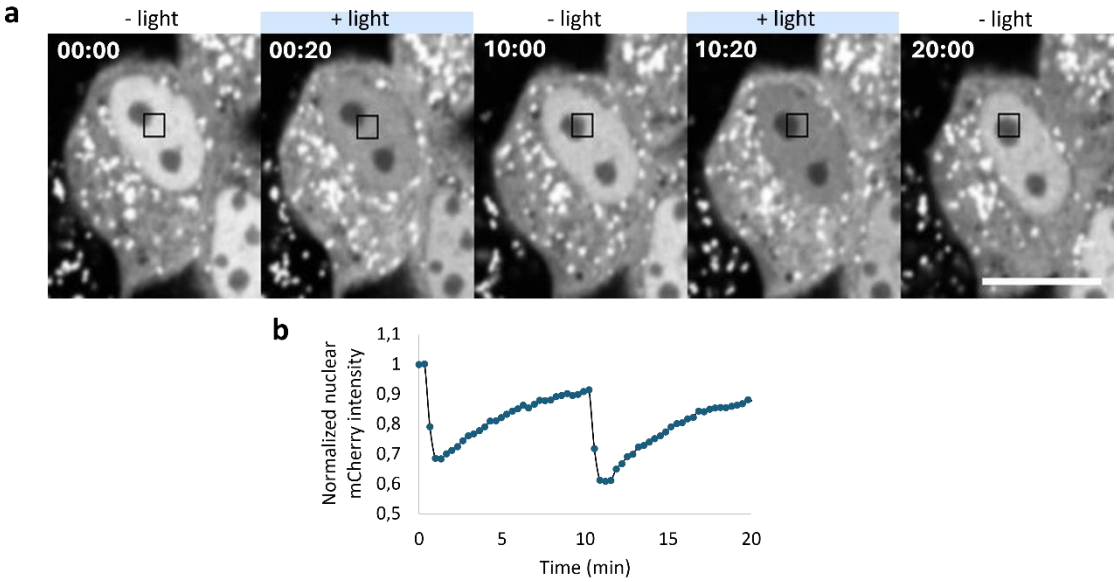

Figure 6 Time-lapse images of photoactivated MDCK II-LEXY cell and mCherry intensity graph during and after activation. a) Transiently transfected MDCK II-LEXY cells were activated with the 458 nm laser for 18 sec. After 10-min dark-state recovery, the stimulation was repeated. ROI =9 μm^2, scale bar 15 µm. Nuclear mCherry intensity graph is shown in b).

5 % of the initial N/C intensity at 25-min and 40-min time points. The corresponding values after the second round of activation were only 76 ± 3 % and 78 ± 6 % (Fig 7e).

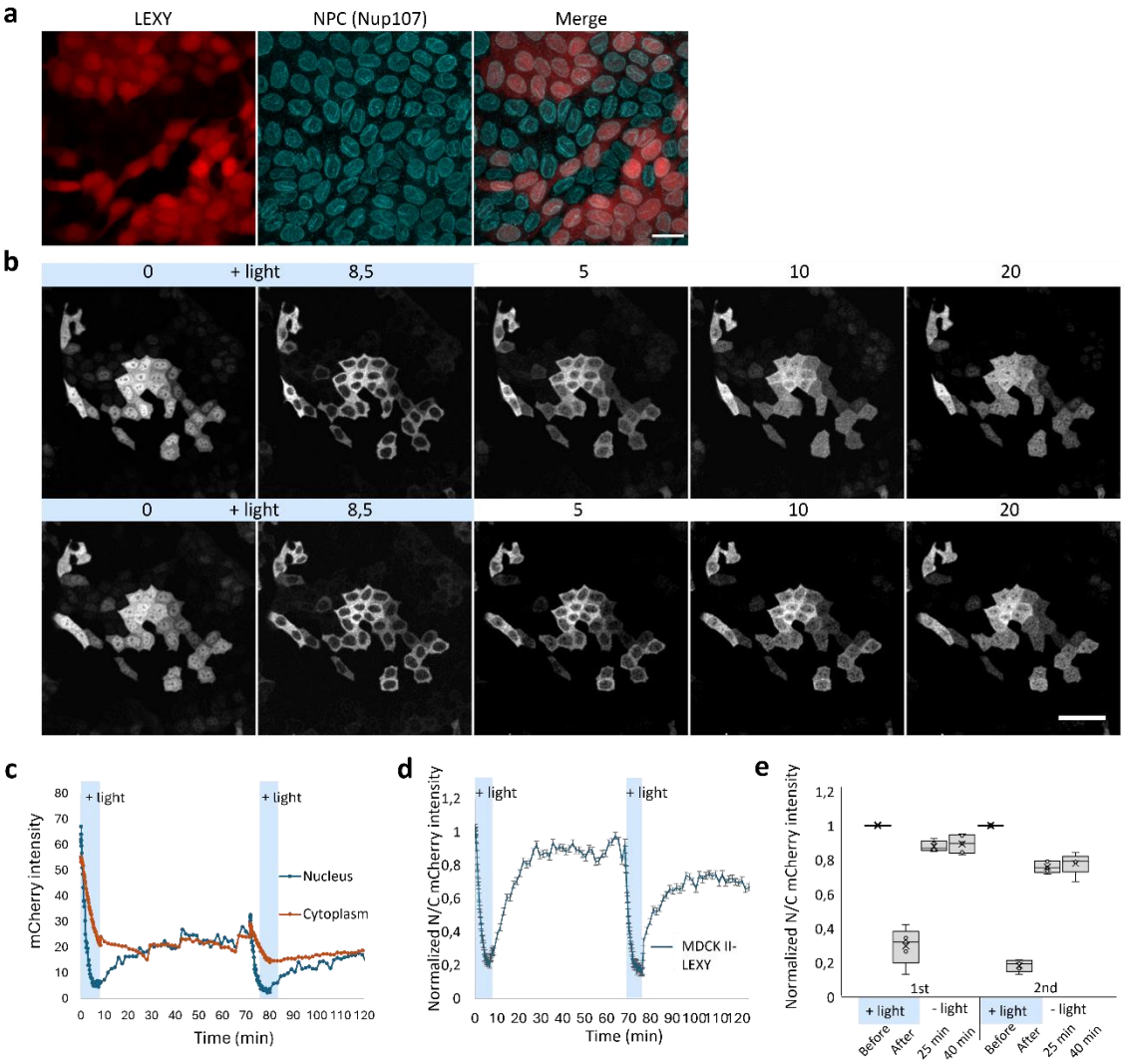

Figure 7. Time-lapse images of MDCK II-LEXY cells and mCherry intensity graphs during and after photoactivations. a) Fixed MDCK II-LEXY cells stained for nucleoporin Nup107, an important NPC protein. Scale bar 20 µm. b) MDCK II-LEXY cells were activated with a 488-laser. Time-lapse shows images of the cells after the 8.5-min stimulation phase and after 5-, 10- and 20-min recovery in the dark state. ROI = 1024 x 1024 pixels, scale bar 50 µm. Nuclear and cytoplasmic mCherry intensity graphs in a single cell are shown in b) and relative N/C mCherry intensity graph of n=5 is shown in c). Relative N/C mCherry intensity graphs (n=5) and relative changes in N/C mCherry intensities before and after the photoactivations are shown in d) and d), respectively.

5.2 Whole-field-of-view stimulations of MDCK II-LEXY cells after cytoskeleton disruption/perturbation

Next, we studied the performance of LEXY before and after the cellular cytoskeleton was disrupted. Perturbation was done using cytoskeleton D and nocodazole. Cytochalasin D is a powerful mycotoxin which inhibits actin polymerization[105], whereas nocodazole is interferes with the structure of microtubules[106]. Since the perinuclear actin cap is known to have an important role in maintaining of the nuclear morphology, inhibition of actin dynamics and these cytoskeletal filaments was hypothesized to result in changed morphology of the nucleus.

We noticed that cytoskeletal perturbation resulted in increased height of the nucleus in MCF7 cells (Fig 8). Similar rounding of the nucleus caused by cytochalasin D treatment has been reported with other epithelial cells such as MCF10-A[107] and MDCK II cells[108].

Activation and imaging of LEXY was done similarly as in the control set-up in whole-field-of-view stimulation. Only this time between the two rounds of imaging, cells were treated with both cytochalasin D and nocodazole for 30 min. After this the activation and imaging were repeated. N/C intensity followed the similar trend as in the case of control cells. After the stimulations, the N/C ratio values dropped to 13 ± 2 % and 21 ± 4% (with drugs) from the baselines. N/C ratio values increased to 88 ± 5 % and 97 ± 7 % of the initial values at 25-min and 40-min time points during the first recovery, respectively, and to 92 ± 4 % and 95 ± 4 % during the second recovery when cells treated with the drugs (Fig 8).

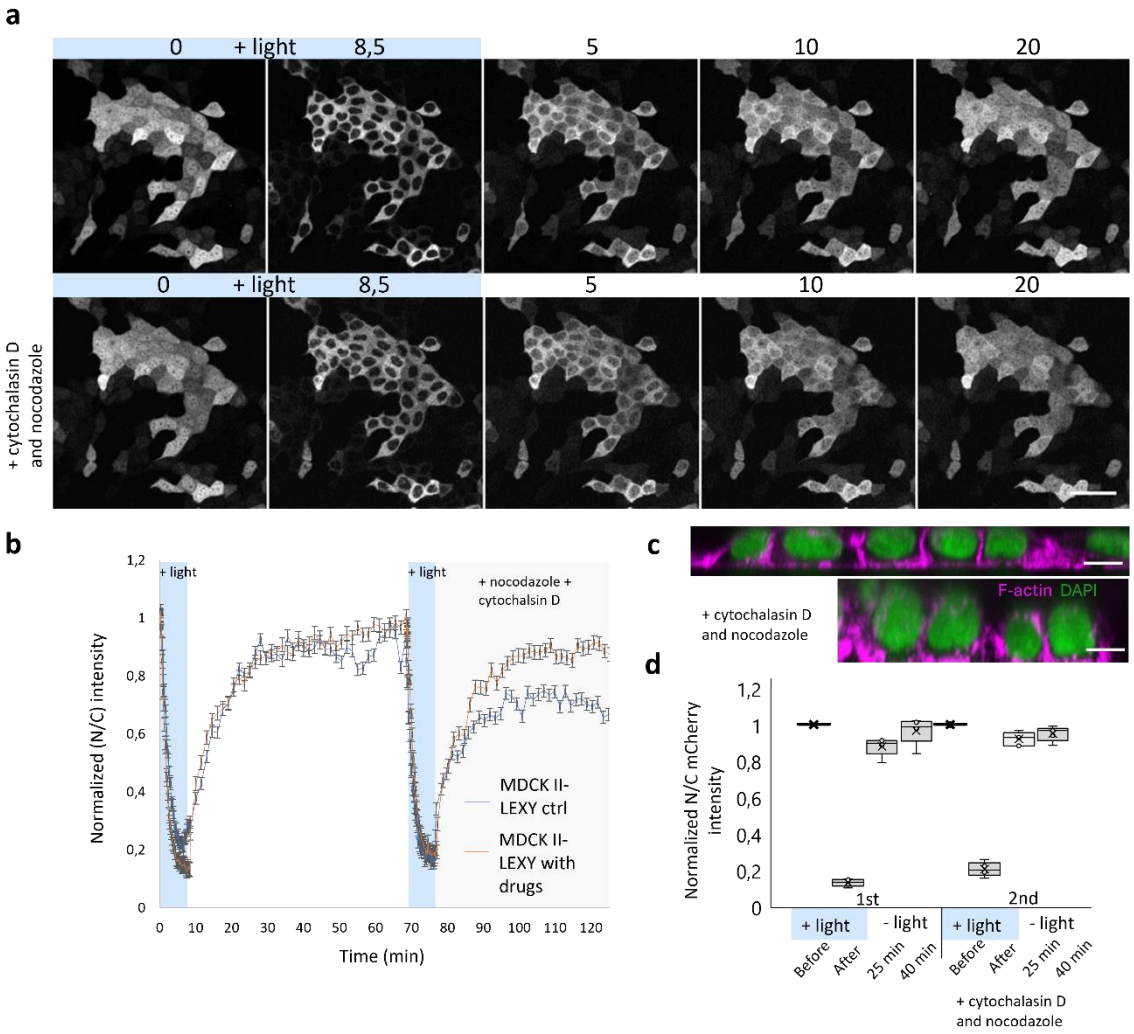

Figure 8 Time-lapse images of photoactivated MDCK II-LEXY cells before and after treating with cytochalasin D and nocodazole. a) MDCK II-LEXY cells were activated with a 488-laser. Time-lapse shows images of the cells after the 8.5-min stimulation phase and after 5-, 10- and 20-min recovery in the dark state. ROI = 1024 x 1024 pixels, scale bar 50 µm. Relative N/C mCherry intensity graph of n=5 is shown in b). c) Nuclei of MCF7 cells before and after a 30-min 10 µg/ml cytochalasin D and 20 µM nocodazole treatment. Scale bar 10 µm. d) Relative changes in N/C mCherry intensities before and after the photoactivations, n=5.

5.3 Whole-field-of-view stimulations of MDCK II-LEXY cells after compression

Next, we wanted to study the effect of nuclear deformation on the LEXY. This was done by adding physical weights on the cells causing squeezing of the cells and nuclei. After the first round of stimulation and recovery, the cells were treated with cytochalasin D to

relax the cells and inhibit the possible actin cytoskeleton remodeling caused by compressive stress. Lighter (2.0 g) and heavier weights (5.8 g) were then placed on top of the cells and after 10 min, the stimulation was repeated.

With the lighter weight, photoactivation was performed otherwise similarly as with control, but less stimulation was required to reach the plateau phase within the nucleus. N/C intensity ratio values dropped to 9 ± 3 % and 20 ± 7% (with lighter weight) from the baselines after stimulations. At 25-min and 40-min timepoints, the N/C intensity increased to 89 ± 4 % and 92 ± 6 % of the initial value, and after the second recovery they had increased 109 ± 15 % and 98 ± 2 % (with lighter weight) (Fig 9d).

With the heavier weight, N/C intensities after stimulations dropped to 13 ± 4 % and 22 ± 2 % (with weight) from the baselines. During the first recovery, N/C intensities increased to 113 ± 33 % and 115 ± 28 % at 25-min and 40-min time points, respectively. With the heavier weight, we were only able to follow the recovery for 25-min before the cells moved out of focus. By then, N/C intensity had increased to 76 ± 12 % (Fig 9d).

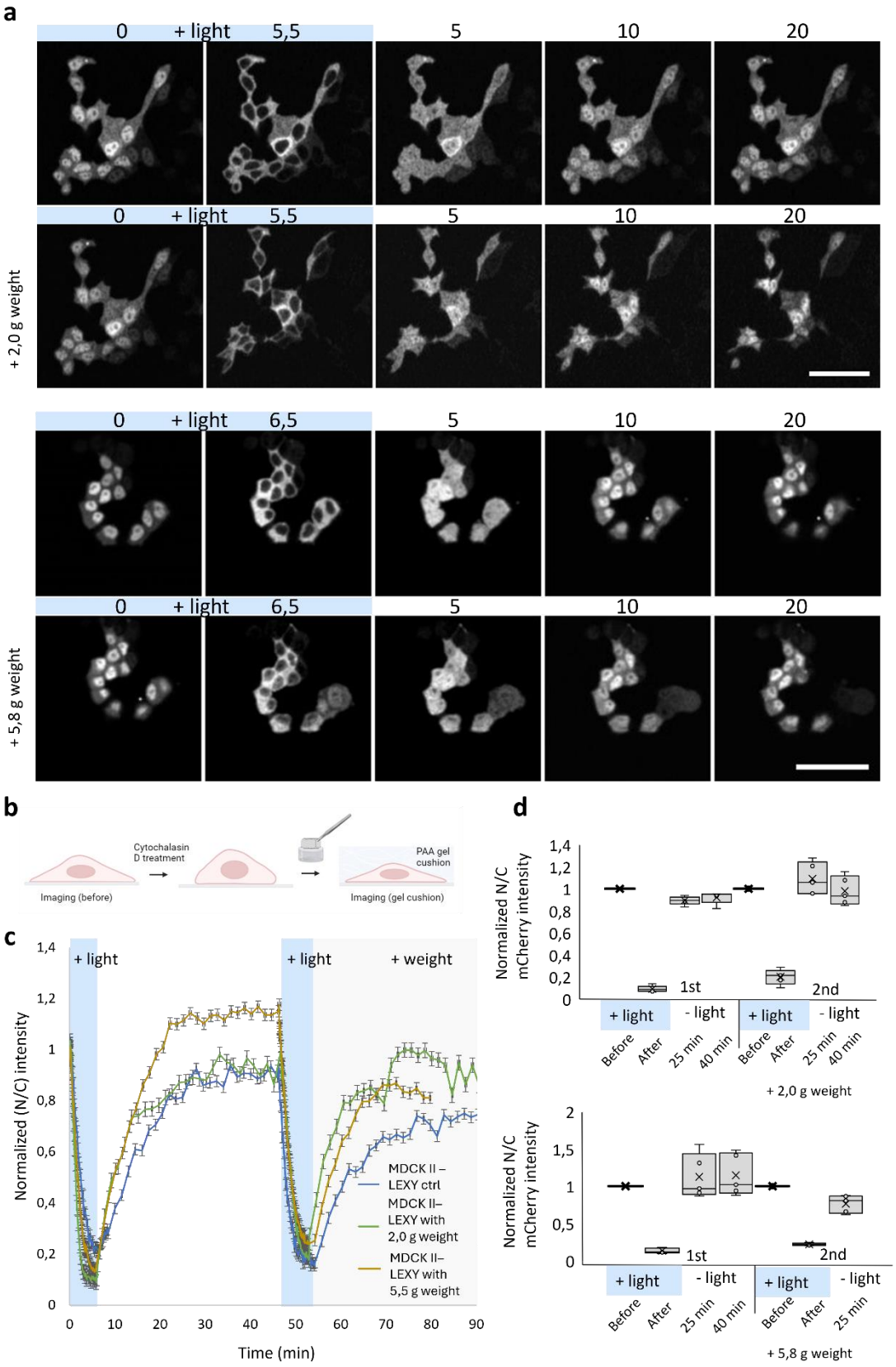

Figure 9 Time-lapse images of photoactivated MDCK II-LEXY cells before and after compressing cells with physical weights. a) MDCK II-LEXY cells were activated with a 488-laser. Time-lapses show images of the cells after the 5.5-min (light weight) or 6.5-min (heavy weight) stimulation phase and at 5-, 10- and 20-min recovery time points. ROI = 1024 x 1024 pixels (light weight), 512 x 512 pixels (heavy weight), scale bars 50 µm. b) Before imaging with the weights, cells were treated with cytochalasin D 10 µg/ml for 30 min. Relative N/C mCherry intensity graphs (n=5) and relative changes in N/C mCherry intensities before and after the photoactivations are shown in c) and d), respectively.

5.4 Whole-field-of-view stimulations of MCF7-LEXY cells

After optimization and testing of the LEXY with MDCK II epithelial cells, we wanted to test its performance with an epithelial-like cell type, MCF7, which is a brest cancer cell line. Since cancer cells experience various different physical forces espcially during invasion and metastasis, they make excellent candidates for studying whether the nucleocytoplasmic transport might be affected by mechanical perturbations. Similar to MDCK II cells, MCF7 cells were shown to form stress fibers when cultured on stiff surface (Fig 10a) and treating the cells with cytochalasin D and nocodazole were shown to cause major disruption of the actin cytoskeleton (Fig 10b).

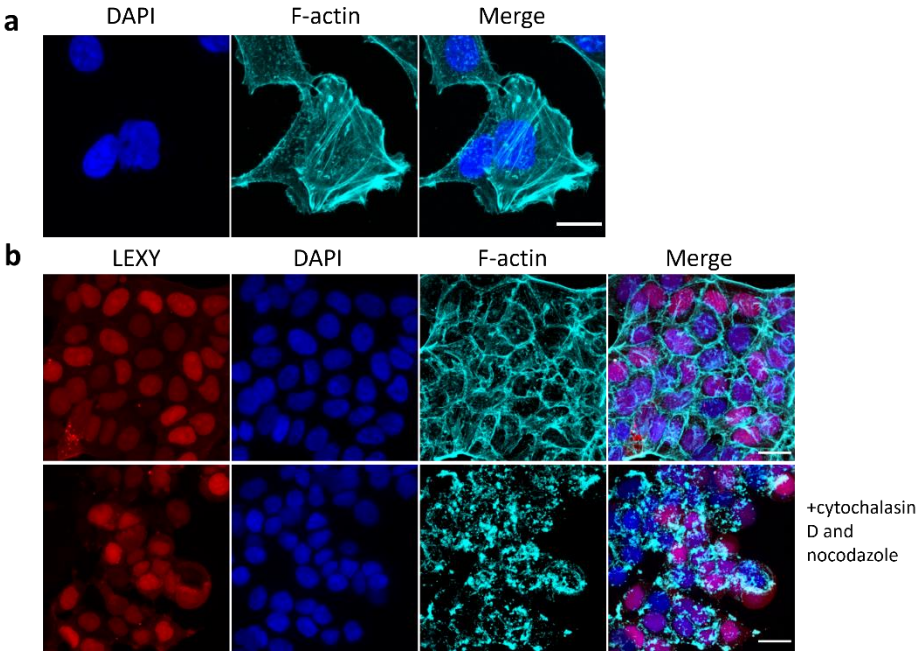

Figure 10 a) Prominent stress fibers in MCF7-LEXY cells seeded and fixed on coverslips. Scalebar 20 µm. b) Immunostainings of fixed MCF7-LEXY cells stained for F-actin before and after a 30-min 10 µg/ml cytochalasin D and 20 µM nocodazole treatment. Scalebar 20 µm.

For MCF7-LEXY cells, the photoactivations were done using a different confocal microscope (Nikon A1R). For all experiments, the microscopy settings were the same. Photoactivation was done with the 488 nm laser (10 % power with ND filter) and the total time of whole-field-of-view stimulation followed by an image capture was only 3.3 min of which blue light exposure was approximately 1.3 min (1.06-sec pulse, 2 iterations, 38 cycles). This illumination regime was shown to be efficient to reach the plateau phase, at which point the N/C ratio values had dropped to 17 ± 3 % and 18 ± 5 % from the baselines after stimulations. The intensity changes during the recovery happened slower compared to those of MDCK II cells; at 25-min and 38-min timepoints, the N/C intensity

increased to 79 ± 13 % and 87 ± 2 % of the initial N/C values, and after the second recovery they had increased to 75 ± 21 % and 81 ± 3 % (Fig 11D).

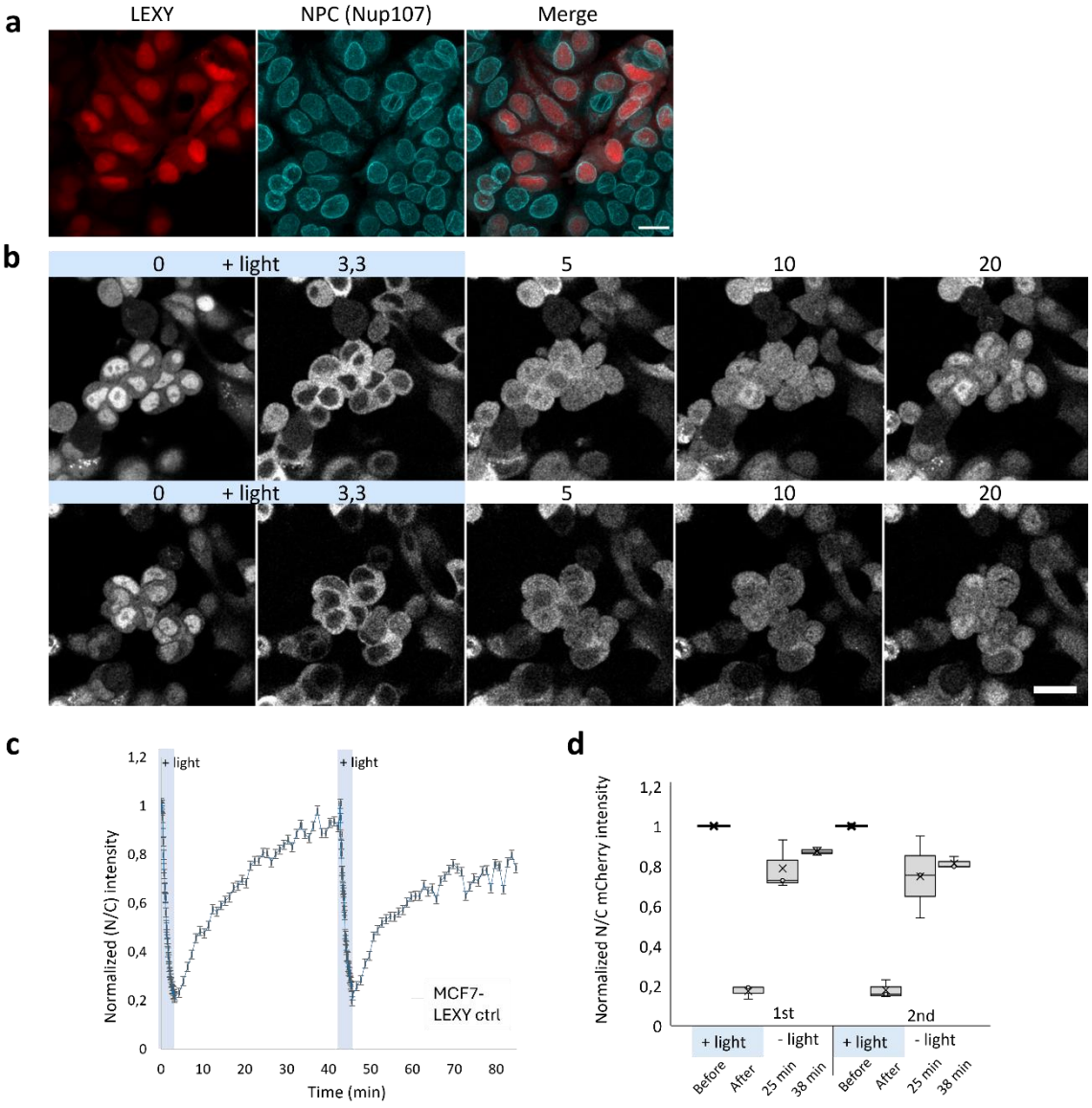

Figure 11 Photoactivation of MCF7-LEXY cells. a) Fixed MCF7-LEXY cells stained for nucleoporin Nup107, an important NPC protein. Scale bar 20 µm. b) Time lapse images of MCF7-LEXY cells before and after stimulation with a 488-laser, and after 5-, 10- and 20-min recovery in the dark state. ROI = 1024 x 1024 pixels, scale bar 25 µm. Relative N/C mCherry intensity graphs (n=3) and relative changes in N/C mCherry intensities before and after the photoactivations are shown in c) and d), respectively.

After the cytoskeletal perturbation, the N/C ratio values dropped to 15 ± 4 % and 19 ± 2 % of the initial N/C intensity, and during the first recovery, it had increased to 74 ± 20 % (at 25 min) and 83 ± 17 % (at 38 min) of the starting N/C intensity. After cytoskeletal perturbation, the N/C intensities at those time points were 90 ± 6 % and 92 ± 16 % (Fig 12).

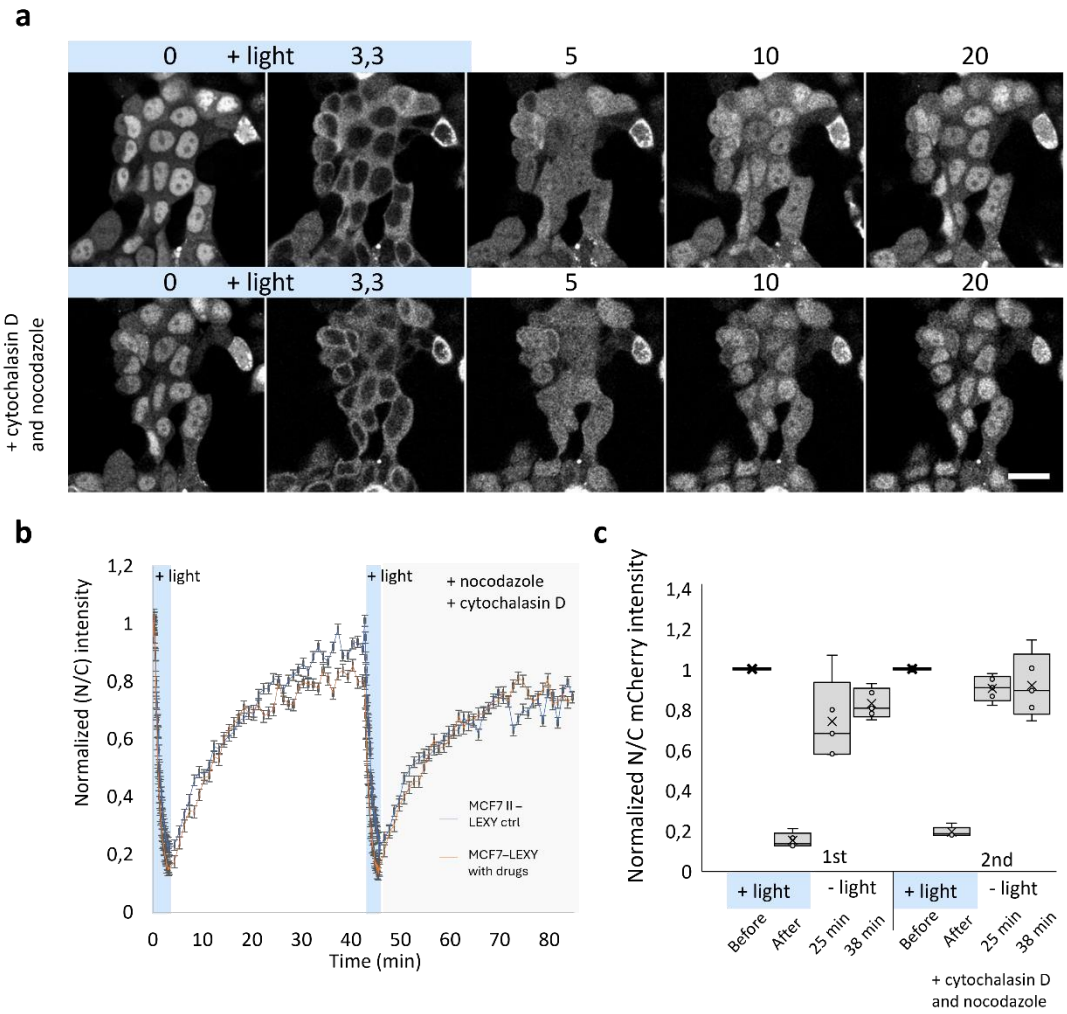

Figure 12 Time-lapse images of photoactivated MCF7-LEXY cells before and after treating with cytochalasin D and nocodazole. a) MCF7-LEXY cells were stimulated with a 488-laser. Time-lapse shows images of the cells after the 3.3-min stimulation phase and after 5-, 10- and 20-min recovery in the dark state. Lower row shows cells after a 30-min 10 µg/ml cytochalasin D and 20 µM nocodazole treatment. ROI = 1024 x 1024 pixels, scale bar 25 µm. Relative N/C mCherry intensity graphs (n=5) and relative changes in N/C mCherry intensities before and after the photoactivations are shown in b) and c), respectively.

Photoactivation with a physical weight was done similarly as with MDCK II cells, and a 5,5 g-weight was placed on the cells before the second round of stimulation. N/C ratio values after stimulations dropped to 15 ± 6 % and 26 ± 9 % from the baselines. During the first recovery, N/C intensities increased to 76 ± 11 % and 94 ± 15 % at 25-min and 40-min time points. Corresponding values were 70 ±14 and 72 ± 7 % after the stimulation with weight (Fig 13C).

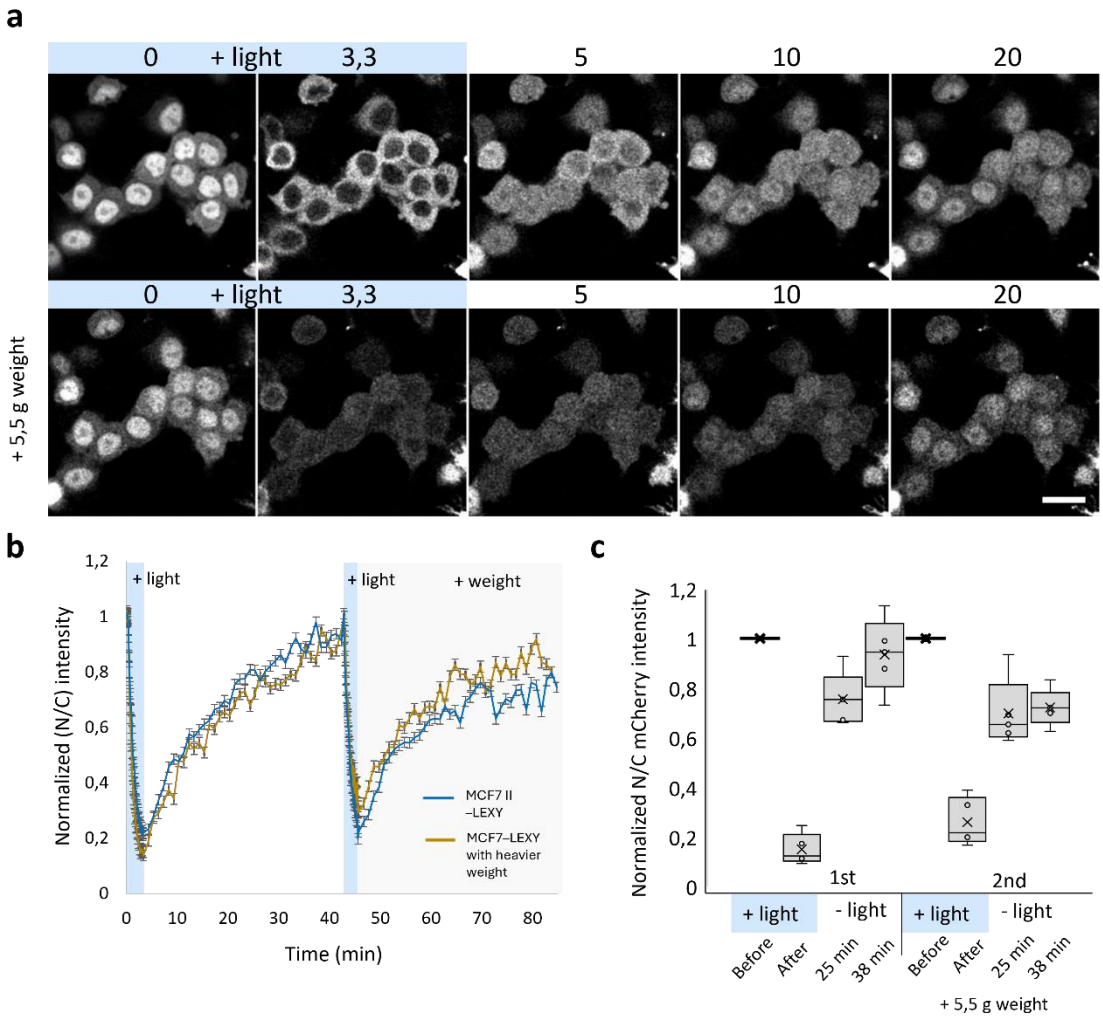

Figure 13 Time-lapse images of photoactivated MCF7-LEXY cells before and after physical compression. a) MCF7-LEXY cells were stimulated with a 488-laser. Time-lapse shows images of the cells after the 3.3-min stimulation phase and after 5-, 10- and 20-min recovery in the dark state. Lower row shows cells after adding the weight. ROI = 1024 x 1024 pixels, scale bar 25 µm. Relative N/C mCherry intensity graphs (n=5) and relative changes in N/C mCherry intensities before and after the photoactivations are shown in b) and c), respectively.

5.5 N/C ratios in the dark state

In the dark state, nuclear-to-cytoplasmic ratio of LEXY showed some variability especially in MDCK II-LEXY cells (Fig 14a). In control cells, the N/C ratios before photoactivations were 1.54 ± 0.327 and 1.260 ± 0.209. Before and after cytoskeletal disruption, the N/C ratios were 1.22 ± 0.205 and 1.12 ± 0.127, respectively. With lighter weight, the N/C ratios were 2.13 ± 0.240 before, and 1.95 ± 0.440 after the weight application. With heavier weight the N/C ratios were 3.03 ± 0.365 and 3.08 ± 0.397, before and after the weight was applied, respectively.

In MCF7-LEXY cells, the N/C ratios showed less variation between samples (Fig 14b). In control cells, the initial N/C ratios were 2.44 ± 0.656 and 2.09 ± 0.665. With drugs, the corresponding values were 2.64 ± 0.760 and 2.70 ± 0.614. With heavier weight, N/C ratios were 2.511 ± 0.460 and 2.74 ± 0.682.

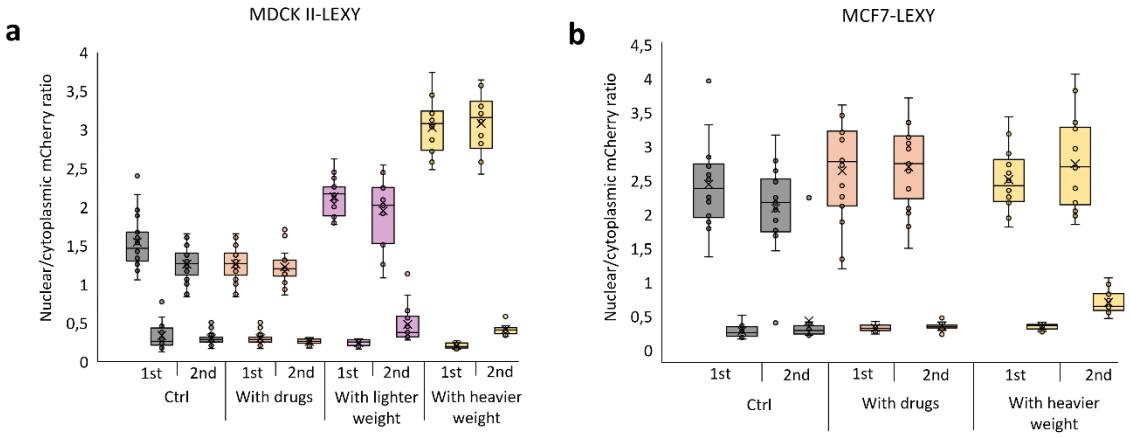

Figure 14 N/C ratios of MDCK II-LEXY and MCF7-LEXY cells. N/C ratios in a) MDCK II-LEXY and b) MCF7-LEXY cells before and after blue-light stimulations in each experiment. N = 10-30

5.6 Curve fitting and kinetic analysis

The activation of the LEXY construct happens very quickly, and the translocation from the nucleus to the cytoplasm is extremely fast related to confocal imaging. For this reason, rather than studying the active transport from nucleus to the cytoplasm during activation, we decided to focus on the nuclear import kinetics during the recovery. To derive quantitative values from the data, we first needed to fit our data to a mathematical model. A good fit ($R^2 > 0.9$) was found with an exponential equation $y(x) = a*(1-e^{(-b*x)})$. With MDCK II-LEXY cells, the first 25 min of the recoveries were used for the fitting as follows: $I_{N/C\ mCherry}(t) = I_{N/C\ mCherry}\ max * (1-e^{-kt})$, where $I_{N/C\ mCherry}\ max$ = mCherry fluorescence intensity at steady-state and t = time. From this equation, the rate constants (k) were derived. Both the graphs of the original data and the fitted data are shown in Figure 14. With MCF7-LEXY cells, datapoints of the whole recovery period (38 min) was used in the curve fitting, since this was the time point when the intensity started to reach a plateau (Fig 15).

With MDCK II-LEXY cells, no significant difference was found between the rate constants (*k)* of control cells and with cells with the lighter compression / weight, but a significant difference was found within groups where the cytoskeleton was disrupted and with the heavier compression. Within control cells, the *k* was 0.11 ± 0.057 1/min during the first

recovery, and 0.13 ± 0.052 1/min during the second recovery. With lighter weight the corresponding values were 0.19 ± 0.019 1/min and 0.19 ± 0.071 1/min. There was a significant increase in *k* with the heavier compression (+0.081 ± 0.025 1/min, p = 0.02) and a significant decrease when the cytoskeleton was disrupted (-0.077 ± 0.056 1/min, p = 0.03).

With MCF7-LEXY cells, no statistically significant difference was found within any of the groups. In control cells, *k* was 0.084 ± 0.013 1/min during the first recovery and 0.089 ± 0.0039 1/min during the second recovery. When the cytoskeleton was disrupted, *k* values were 0.095 ± 0.013 1/min and 0.094 ± 0.021 1/min during the first and second recoveries, respectively. There was some but not statistically significant difference between *k* values within the group of heavier weight. During the first recovery *k* was 0.058 ± 0.011 1/min and during the second recovery *k* was 0.066 ± 0.0064 1/min. Rate constants of both cells lines in each experimental setting are shown in Figure 16.

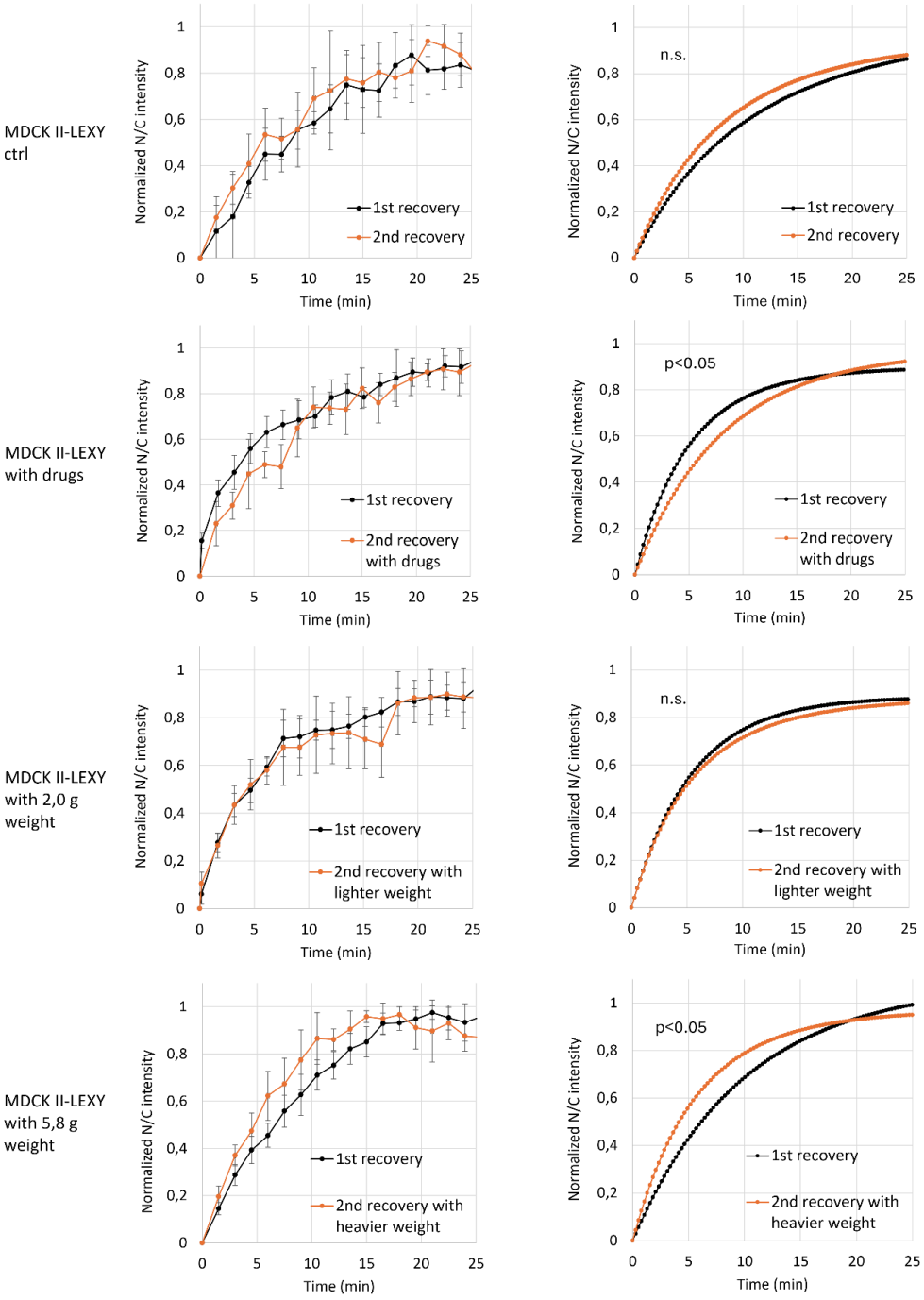

Figure 15 Curve fittings of the data with MDCK II-LEXY cells. Left panel shows original data during the 25-min recoveries. Right panel shows the data after fitting to an exponential function $I_{N/C}(t) = I_{N/C}max * (1-e^{-kt})$. N=5 in all sets.

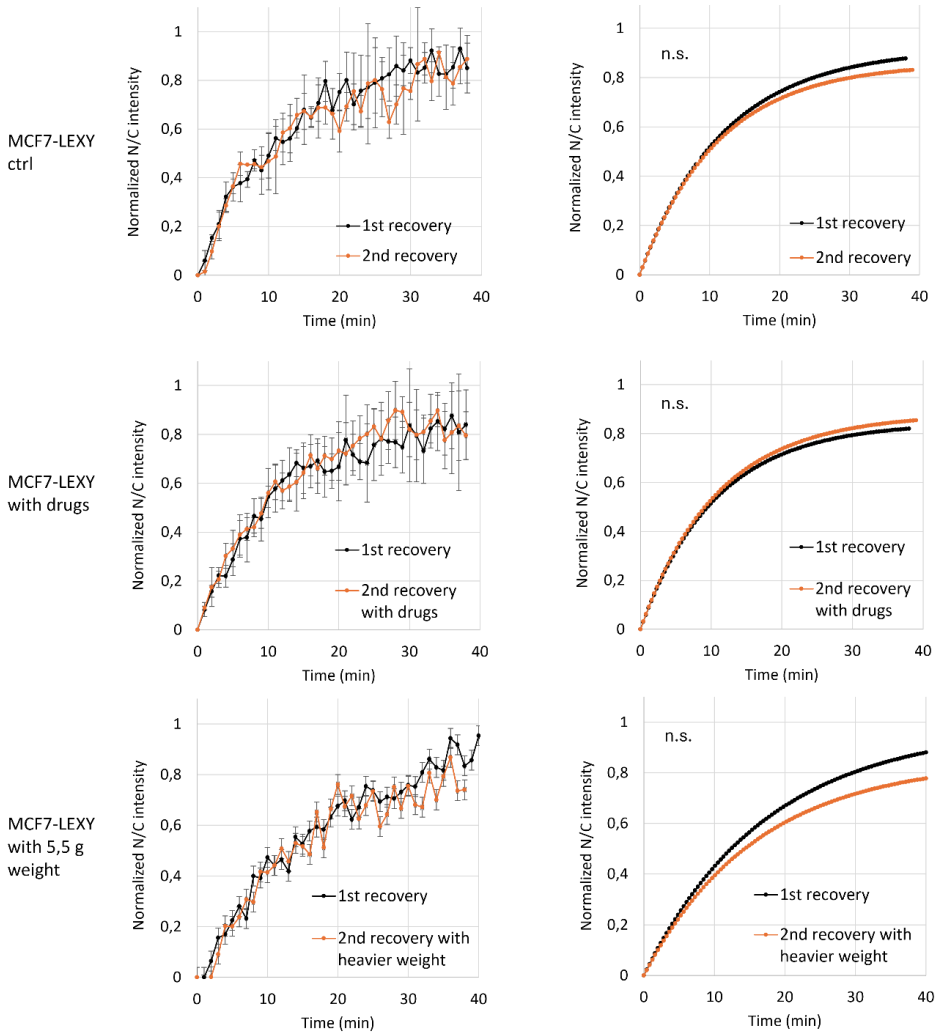

Figure 16 Curve fittings of the data with MCF7-LEXY cells. Left panel shows original data during the 40-min recoveries. Right panel shows the data after fitting to an exponential function $I_{N/C}(t) = I_{N/C}max * (1-e^{-kt})$. N=5 in all sets except for control, where n=3.

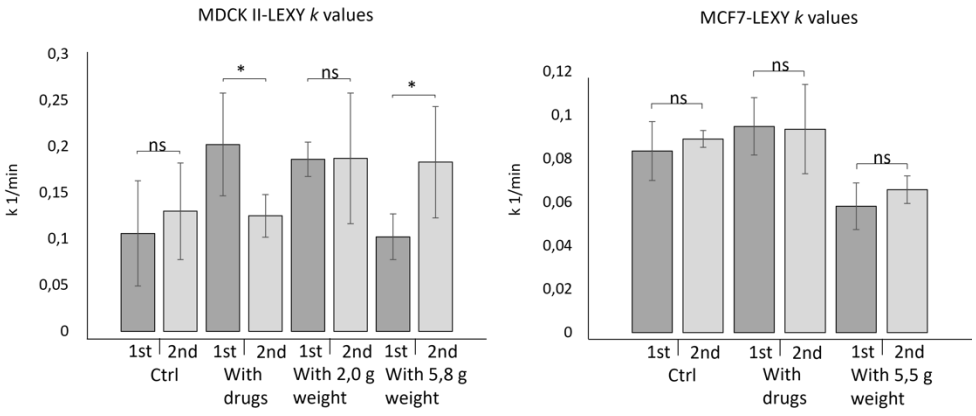

Figure 17 K-values derived from the fitted recovery data. Bar graphs show the rate constants of the same cells during both recoveries. Higher rate constant indicates faster translocation of the LEXY to the nucleus after photoactivation. Left figure shows rate constants of MDCK II-LEXY cells and right figure shows those of MCF7-LEXY cells. N=5 in all but MCF7-LEXY ctrl cells, where n=3. * $p < 0.05$.

6. DISCUSSION

6.1 LEXY's performance

Our results demonstrated that the LEXY system was successfully implemented and functional in both MDCK II and MCF7 cell lines. By using confocal microscopes, we achieved targeted activation of the construct in both individual cells as well as in specific groups of cells in monolayers. Activation of the construct could be performed in repeated cycles of activation and reversion without much effect on LEXY's functionality or having drastic effects on cellular viability. Although the absolute light intensities were not measured, we were able to activate the system using different relative levels of stimulations. The high dynamic range was also indicated by the large changes in N/C intensity ratio before and after the blue-light stimulation. Our results therefore support the statement that LEXY has a relatively high dynamic range.

Overall, LEXY maintained its responsiveness over multiple rounds of stimulation. In general, following blue-light stimulation, the N/C ratios dropped to at least 22 % of the baseline values; however, the extent of this drop diminished after the second stimulation, especially in MDCK II cells. In most cases, the construct also did not exhibit a full 100 % recovery, but the N/C ratio was lower after each recovery phase. Given that LEXY is reported to show full recovery within about 15 min in the dark[5], our 25- and 40-min recovery periods should have be sufficient. This incomplete recovery might be explained by the fact, that the construct does not fully return to its original conformational state after the stimulation, leading to dark state leakage. Additionally, repeated light stimulation may also gradually alter its conformational states over time.

The performance of the LEXY can be further optimized to suit specific research needs. For instance, mutated variants such iLEXY[109] have been developed to enhance functionality under different conditions. iLEXY demonstrated better fold change between light and dark states with lower light intensity, but it has increased leakiness in the resulting in reduced N/C localization in the dark state. This variant can be beneficial when aiming to deplete the nucleus entirely of the POI, as seen with the transcription factor Twist. In contrast, the original LEXY has minimal leakiness and would be more suitable in the case when the POI is known to have any cytoplasmic activity, allowing it to remain in the nucleus in the dark state.

6.2 Single-cell vs whole-field-of-view activations

The illumination regimes used in this work were quite different compared to those of previous studies in both single cells and whole-field-of-view activations. In general, other groups have used longer intervals in both blue-light illumination and image capturing. In the original LEXY study by Niopek et al[5], single cell activations were performed with a 458 nm laser for 30 ms every 10 s for 10 min resulting in 1.8-sec illumination. In contrast, we used the 458 nm laser with 362 ms pulses over 50 cycles resulting in cumulative illumination time of 18.1 sec. For whole-field-of-view activations, Niopek et al applied the 458 nm laser every 30 s for 40 min, whereas we achieved an effective response with the 488 nm laser with repeated 9.6-sec blue light pulses for 5.5 – 8.5 min in MDCK II cells, and 2.1-sec pulses over 3.3 min in MCF7 cells. Thus, our illumination times were substantially shorter for both single-cell and whole-field-of-view activations.

Comparing illumination regimes and LEXY's performance across different studies can be insightful, but these comparisons require careful considerations due to the substantial impact of experimental conditions on outcomes. Differences in light delivery systems, such as lasers versus LEDs, and in optical setups, can alter the effective light intensity, duration, and distribution at the cellular level. Since each study might have a different experimental goal, this can further influence the illumination protocols. Additionally, cell types might vary in their responses to identical illumination regimes and LEXY can exhibit different behavior depending on the cell type. Cell lines used in Niopek's study also differed from those in our experiments. Furthermore, our results also showed that the cell type might play an important role in LEXY optimization, albeit two different confocal microscopes were used. The initial N/C ratio of LEXY also seemed to vary even within and between cell populations especially in MDCK II cells. This high heterogeneity might be explained with for example different copy numbers of the construct or variability in expression levels.

Although whole-field-of-view activations allow for simultaneous observation of multiple cells, it also leads to greater and more widespread photobleaching. Since photobleaching was a significant issue in our relatively long whole-field-of-view experiments, increasing the intervals between pulses and mCherry imaging could help reduce photobleaching and improve signal, making quantitative analyses more reliable. Since with single cells the laser can be focused on a smaller area, the overall exposure is usually diminished.

Extending the intervals between laser pulses would further help minimize cytotoxic effects, although cells generally tolerated the more frequent illumination well in our experiments. Overall, the interval timing of laser pulses could still be further optimized, especially for experiments requiring multiple rounds of stimulation over extended periods.

6.3 Nuclear compression appears to accelerates import, while cytoskeletal disruption slows it in MDCK II cells

According to our results, the import of LEXY seemed to occur faster under nuclear compression in MDCK II cells, but only with the application of a heavier weight. In contrast, the import seemed to be slower with disrupted cytoskeleton. At least two previous studies support our findings.

Andreu et al (2022) studied the nucleocytoplasmic transport of LEXY in mouse embryonic fibroblasts under mechanical perturbations. In their study, the mechanical environment was controlled by altering substrate stiffness. Their findings showed that increased substrate stiffness resulted in greater changes in the N/C rates. They also observed higher initial N/C ratios of LEXY in cells on stiffer substrate. Since the NLS is dominant in the dark state, an N/C ratio greater than 1 suggests that active import of LEXY is enhanced on stiffer substrate, as more LEXY accumulates in the nucleus. Additionally, they observed that force application to the nucleus in cells seeded on soft substrate increased N/C ratios but only when an NLS was present. This setup could theoretically resemble our own setup with weights, where the nucleus initially appeared relaxed and had more rounded (cytochalasin D vs soft substrata), followed by force application (PAA gel vs atomic force microscopy (AFM)). However, our results did not show a significant increase in the N/C ratio after weight application. This discrepancy could be partially explained by the fact, that in our experiments with heavy weight, the initial N/C ratios were already relatively high compared to control cells. In general, there is a practical upper limit to the N/C ratio of proteins, influenced by factors such as nuclear size and the capacity of the nuclear import machinery[110], which could explain this result.

In another study, the same group showed that force application to the nucleus also accelerated passive diffusion. Using the same AFM technique, they showed that force application caused the well-known force-responsive transcription factor YAP to translocate from the cytoplasm to the nucleus, increasing the N/C ratio of YAP. In addition, treatment with cytochalasin D reduced YAP nuclear localization, but effect was reversed with force

application. These findings align with our results, since the recovery of LEXY was observed to be slower upon cytochalasin D treatment and faster upon nuclear compression. Given that AFM applies force to individual cells, while compression using a PAA gel cushion affects larger regions within cell monolayers, our approach could better replicate cellular behaviors as they might occur in vivo. However, force application may potentially alter the shape of the LEXY construct and impact its rate of passive diffusion. Thus, it is difficult to determine the extent to which our results can be explained by changes in passive or/and facilitated transport.

The group hypothesized that these changes in nuclear transport could be primarily explained by nuclear deformations and flattening, leading to conformational changes in the NPCs. In practice, force application increases tension across the nuclear membrane and thereby increases its curvature. The resulting lateral forces within the nuclear membrane partially open the pores and lower the permeability barrier of NPC. In fact, several studies support this theory[14,111,112]. Specifically, the group suggests that force could enhance nuclear pore exposure to the cytosolic side of the membrane favoring import over export. Altogether, they propose that nuclear force weakens the NPC permeability barrier, thereby increasing diffusion. Similarly, nuclear pore dilation and constriction in response to osmotic pressure changes are thought to result from altered nuclear membrane tension[14]. According to this model, excess of membrane generated by nuclear shrinkage during osmotic shock would reduce tension and lead to NPC constriction, and vice versa.

Our findings also support the proposed direct regulation of NPC permeability by nuclear membrane tension. In our study, the 40-min force application can be considered relatively short-term, likely not leading to large-scale transcriptional responses within this time frame. Since the nuclear import was observed only to accelerate in the case of heavier weight but not with the lighter weight, this difference could simply be reasoned to be dependent on the magnitude of nuclear deformation. The possible mild deformations resulted from the lighter weight application may not have been sufficient to significantly impact nuclear membrane curvature and nuclear pore function. Whereas with heavier compression, the nuclear flattening and deformation could have been more significant thereby enhancing nuclear import by altering nuclear pore conformation. Since the cytoskeleton was disrupted with cytochalasin D, and the stabilizing effects of the cytoskeleton and cell-cell adhesions are unlikely to have influenced the results.

A very recent study has reported that the rates of nucleocytoplasmic transport (NCT) are primarily driven by differences in GTP availability rather than by the mechanical state of

the nucleus[113]. Since the GTP/GDP gradient is an important driving factor of the NCT, many energy-dependent cellular processes can influence this gradient. Interestingly, they reported opposite results of those reported by Andreu et al, despite using similar methods. For example, perturbation of the LINC complex led to an increase in GTP levels and NCT rates, in contrast to the findings reported by Andreu et al. Additionally, depolymerization of the cytoskeleton increased GTP availability resulting in increase in rate of NCT, which contrasts with the results of our study.

We cannot rule out the possible differences in cellular context affecting the rates of NCT across different cell types. For instance, Andreu et al. used primary mouse fibroblasts (MEF), while Scott et al. used BJ-5ta immortalized human fibroblasts, which likely have very different genetic and epigenetic profiles. Thus, they might utilize different mechanotranduction pathways leading to varying cellular responses to stimuli such as mechanical stress. Therefore, differences between the studies could be partially explained by the species-specific and cell-type-specific variations in NCT machinery, nuclear envelope integrity, and cytoskeletal structure[84]. Furthermore, since all the studies discussed here used different cell lines compared to the ones in our experiments, these comparisons should be made with caution.

6.4 Mechanical perturbations do not directly affect import rates in MCF7 cells

In contrast to MDCK II cells, the MCF7 cells showed no differences in NCT rates of LEXY under mechanical perturbations. While a similar trend of accelerated nuclear import of LEXY was observed in MCF7 cells, as seen with MDCK II cells, the change was not statistically significant.

Several factors, particularly the cell type, may account for these findings. Cancer cells, especially invasive cell lines. are known to exhibit a more deformable and less mechanically stable cell structure[82,113]. Although MCF7 cells are generally classified as non- or low-invasive[114,115], there is some conflicting evidence on the deformability of their nuclei. For example, one study reported that MCF7 nuclei remained almost unaffected following a hyperosmotic shock or cytoskeletal disruption, implicating a tighter nuclear architecture and stiffness[114]. On the other hand, the nuclei of MCF7 cells have been reported to ex-

hibit higher deformability mainly due to lower expression of lamin A[116]. In our experiments, however, we observed a significant nuclear deformation in MCF7 nuclei after cytoskeletal disruption.

Therefore, it might be that other factors beyond nuclear deformation have a more significant impact on NCT rates in MCF7 cells. These factors could include the heterogeneity and uneven distribution of nuclear pores in the nuclear membrane, the availability of nuclear transport receptors, and the nucleocytoplasmic Ran gradient, all of which have been reported to play a role in NCT[25,32]. In addition, the nuclear transport machinery itself is regulated, for example, by the cell cycle[117]. Overall, changes in transport rates could result from a joint action of all these factors and those previously discussed. Yet, the interpretation of what drives the changes, and the contribution of each component is often complicated. Given that LEXY can enter the nucleus through both passive and facilitated diffusion, this further complicates the interpretation of our results. Therefore, additional replications are needed to confirm our findings before drawing further conclusions.

6.5 Sources of error and limitations of the study

As previously mentioned, the LEXY system may not perform consistently across all cell types due to various factors already discussed, which can impact both the interpretation and generalizability of the results. In addition, LEXY system has several technical limitations that can influence experimental outcomes.

While the LEXY system has been shown to perform well and maintain resilience through multiple rounds of activation and deactivation, the two rounds of stimulation in our experiments could have influenced the results. Repeated photoactivation is likely to increase phototoxicity, as blue light is known to cause cellular damage and alter cell behavior[102]. Moreover, insufficient recovery time between the activations could lead to a situation where the construct is not fully reversed, possibly leading to incomplete or reduced responsiveness in subsequent rounds. Although the recovery times used in our study were generally longer than those reported in previous studies, the MCF7-LEXY cells were unable to reach a plateau in N/C intensity values within 40-min of recovery.

There is also the possibility that the use of different confocal microscopes and illumination settings may have influenced the results to some extent. Since we did not measure

the absolute light intensities used, the overall dose of blue light likely varied across experiments, which could lead to differences in the degree and duration of LEXY activation. This variability could affect the reliability of results. Therefore, careful calibration of light exposure and timing between activations should be further optimized to help sustain LEXY's performance across multiple rounds of activations.

Since LEXY relies on fluorescence markers for tracking and visualization, factors such as photobleaching reduces the fluorescence signal, making it harder to monitor the nucleocytoplasmic movement accurately. The photobleaching also diminishes the clarity and contrast of the signal especially in the whole-field-of view activations, which therefore can distort quantitative measurements. Since we did not make any image analysis corrections for photobleaching, this would be highly recommended to improve data accuracy.

Additionally, some limitations arise in the curve fitting approach used to assess LEXY's performance. It is important to point out, that the exponential fit used it is a very simplified model of LEXY's import kinetics. Both passive and facilitated diffusion take place during the recovery phase, both of which have different rate constants. In our model, $I_{N/C\ mCherry}(t) = I_{N/C\ mCherry}\,max * (1-e^{-kt})$, the rate constant describes the overall import rate of LEXY. Although this model has been applied in other nucleocytoplasmic transport studies, including for LEXY, alternative or more complex models might provide more accurate insights into LEXY kinetics.

From an experimental point of view, it would have been beneficial to assess LEXY's performance by applying mechanical perturbations in fresh, unperturbed cells. Since in our study mechanical perturbations were introduced only after the first round of LEXY activation and recovery, possibly influencing the baseline transport dynamics due to prior exposure. In future studies, it would also be beneficial to include blue light-only control experiments in samples without the optogenetic protein to help distinguish the effects of light exposure from the optogenetic activation itself.

7. CONCLUSIONS

Our study demonstrated that the LEXY system was successfully implemented and functional in both MDCK II and MCF7 cell lines, with the construct remaining responsive to repeated cycles of activation and reversion without significantly affecting cellular viability. This could be achieved with both single-cell and whole-field-of-view activations with a confocal microscope. Since a confocal microscope allows for a specially restricted activation of the LEXY system, it is possible to investigate how the activation in one cell may influence the behavior of its neighboring cells.

The system exhibited a high dynamic range, as indicated by substantial changes in the N/C ratio before and after blue-light stimulation. Although complete recovery was not always achieved, LEXY showed consistent performance across multiple stimulations. The variability in cell responses and expression levels, along with challenges such as photobleaching in long-duration experiments, highlight the need for optimization of pulse intervals and imaging timing for more reliable quantitative analysis, especially in extended experiments.

Our study showed that LEXY import in MDCK II cells was accelerated under nuclear compression, but only with heavier weight, while cytoskeleton disruption slowed import. These results align with previous studies suggesting that mechanical perturbations, such as force application, can affect nuclear import by altering nuclear membrane tension and NPC permeability. However, discrepancies with other studies, such as differences in N/C ratios and the role of GTP availability, highlight the complexity of nucleocytoplasmic transport and the importance of cell-type-specific factors. Further investigation is needed to fully understand the interplay between mechanical forces and transport dynamics. MCF7-LEXY cells showed no significant change in nuclear transport (NCT) rates under mechanical perturbations, unlike MDCK II-LEXY cells. This difference may be due to factors such as the less deformable nature of MCF7 cells, variations in nuclear pore distribution, transporter availability, and the Ran gradient. In all, these findings underscore the need for further research to fully understand the interplay between mechanical forces, nuclear transport, and cell-specific factors.

In general, LEXY appears to be a promising tool to be used in mechanobiological studies and more particularly in contexts where nucleocytoplasmic transport dynamics play a

role. In future studies, LEXY could be attached to a mechanoresponsive transporter such as YAP, allowing precise modulation of its activity in response to mechanical signals. This could be especially interesting given the importance of mechanical forces in regulating YAP's behavior in various cancer cell types and tissues.

8. REFERENCES

1. Ruppel, A. *et al.* Force propagation between epithelial cells depends on active coupling and mechano-structural polarization. *eLife* **12**, e83588 (2023).
2. Ribbeck, K. & Görlich, D. Kinetic analysis of translocation through nuclear pore complexes. *The EMBO Journal* **20**, 1320 (2001).
3. Yang, W., Gelles, J. & Musser, S. M. Imaging of single-molecule translocation through nuclear pore complexes. *Proc Natl Acad Sci U S A* **101**, 12887–12892 (2004).
4. Pastrana, E. Optogenetics: controlling cell function with light. *Nat Methods* **8**, 24–25 (2011).
5. Niopek, D., Wehler, P., Roensch, J., Eils, R. & Ventura, B. D. Optogenetic control of nuclear protein export. *Nature Communications* **7**, (2016).
6. Hampoelz, B., Andres-Pons, A., Kastritis, P. & Beck, M. Structure and Assembly of the Nuclear Pore Complex. *Annu Rev Biophys* **48**, 515–536 (2019).
7. Dultz, E., Wojtynek, M., Medalia, O. & Onischenko, E. The Nuclear Pore Complex: Birth, Life, and Death of a Cellular Behemoth. *Cells* **11**, 1456 (2022).
8. Cautain, B., Hill, R., de Pedro, N. & Link, W. Components and regulation of nuclear transport processes. *FEBS J* **282**, 445–462 (2015).
9. Sakuma, S. & D'Angelo, M. A. The roles of the nuclear pore complex in cellular dysfunction, aging and disease. *Semin Cell Dev Biol* **68**, 72–84 (2017).
10. Coyne, A. N. & Rothstein, J. D. Nuclear pore complexes — a doorway to neural injury in neurodegeneration. *Nat Rev Neurol* **18**, 348–362 (2022).
11. Hung, M.-C. & Link, W. Protein localization in disease and therapy. *Journal of Cell Science* **124**, 3381–3392 (2011).
12. Hill, R., Cautain, B., Pedro, N. de & Link, W. Targeting nucleocytoplasmic transport in cancer therapy. *Oncotarget* **5**, 11–28 (2013).

13. Kim, S. J. *et al.* Integrative Structure and Functional Anatomy of a Nuclear Pore Complex. *Nature* **555**, 475–482 (2018).
14. Zimmerli, C. E. *et al.* Nuclear pores dilate and constrict in cellulo. *Science* **374**, 1341–1341 (2021).
15. Raices, M. & D'Angelo, M. A. Nuclear pore complex composition: a new regulator of tissue-specific and developmental functions. *Nat Rev Mol Cell Biol* **13**, 687–699 (2012).
16. Beck, M. & Hurt, E. The nuclear pore complex: understanding its function through structural insight. *Nat Rev Mol Cell Biol* **18**, 73–89 (2017).
17. Akey, C. W. *et al.* Comprehensive structure and functional adaptations of the yeast nuclear pore complex. *Cell* **185**, 361-378.e25 (2022).
18. Capelson, M. & Hetzer, M. W. The role of nuclear pores in gene regulation, development and disease. *EMBO Rep* **10**, 697–705 (2009).
19. Hoogenboom, B. W. *et al.* Physics of the Nuclear Pore Complex: Theory, Modeling and Experiment. *Phys Rep* **921**, 1–53 (2021).
20. Cowburn, D. & Rout, M. Improving the hole picture: towards a consensus on the mechanism of nuclear transport. *Biochem Soc Trans* **51**, 871–886 (2023).
21. Mosalaganti, S. *et al.* AI-based structure prediction empowers integrative structural analysis of human nuclear pores. *Science* **376**, eabm9506 (2022).
22. Soheilypour, M., Peyro, M., Jahed, Z. & Mofrad, M. R. K. On the Nuclear Pore Complex and Its Roles in Nucleo-Cytoskeletal Coupling and Mechanobiology. *Cel. Mol. Bioeng.* **9**, 217–226 (2016).
23. Raices, M. & D'Angelo, M. A. Nuclear pore complexes and regulation of gene expression. *Curr Opin Cell Biol* **46**, 26–32 (2017).
24. Sun, J., Shi, Y. & Yildirim, E. The Nuclear Pore Complex in Cell Type-Specific Chromatin Structure and Gene Regulation. *Trends in Genetics* **35**, 579–588 (2019).
25. Knockenhauer, K. E. & Schwartz, T. U. The Nuclear Pore Complex as a Flexible and Dynamic Gate. *Cell* **164**, 1162–1171 (2016).

26. Matsuda, A. & Mofrad, M. R. K. On the nuclear pore complex and its emerging role in cellular mechanotransduction. *APL Bioeng* **6**, 011504 (2022).

27. Hs, Y., Yj, O., Ej, L., Ss, K. & Sh, H. Development of a novel DsRed-NLS vector with a monopartite classical nuclear localization signal. *3 Biotech* **9**, (2019).

28. Paci, G., Caria, J. & Lemke, E. A. Cargo transport through the nuclear pore complex at a glance. *J Cell Sci* **134**, jcs247874 (2021).

29. Tu, L.-C., Fu, G., Zilman, A. & Musser, S. M. Large cargo transport by nuclear pores: implications for the spatial organization of FG-nucleoporins. *EMBO J* **32**, 3220–3230 (2013).

30. Di Ventura, B. & Kuhlman, B. Go in! Go out! Inducible control of nuclear localization. *Curr Opin Chem Biol* **34**, 62–71 (2016).

31. Xu, L. & Massagué, J. Nucleocytoplasmic shuttling of signal transducers. *Nat Rev Mol Cell Biol* **5**, 209–219 (2004).

32. Lu, J. *et al.* Types of nuclear localization signals and mechanisms of protein import into the nucleus. *Cell Commun Signal* **19**, 60 (2021).

33. Tran, E. J. & Wente, S. R. Dynamic Nuclear Pore Complexes: Life on the Edge. *Cell* **125**, 1041–1053 (2006).

34. Tago, K., Tsukahara, F., Naruse, M., Yoshioka, T. & Takano, K. Regulation of nuclear retention of glucocorticoid receptor by nuclear Hsp90. *Mol Cell Endocrinol* **213**, 131–138 (2004).

35. Mohr, D., Frey, S., Fischer, T., Güttler, T. & Görlich, D. Characterisation of the passive permeability barrier of nuclear pore complexes. *EMBO J* **28**, 2541–2553 (2009).

36. Infante, E. *et al.* The mechanical stability of proteins regulates their translocation rate into the cell nucleus. *Nat. Phys.* **15**, 973–981 (2019).

37. Colwell, L. J., Brenner, M. P. & Ribbeck, K. Charge as a selection criterion for translocation through the nuclear pore complex. *PLoS Comput Biol* **6**, e1000747 (2010).

38. Ivic, N. *et al.* Fuzzy Interactions Form and Shape the Histone Transport Complex. *Molecular Cell* **73**, 1191-1203.e6 (2019).

39. Wagstaff, K. M. & Jans, D. A. Importins and beyond: non-conventional nuclear transport mechanisms. *Traffic* **10**, 1188–1198 (2009).

40. Elosegui-Artola, A. *et al.* Force Triggers YAP Nuclear Entry by Regulating Transport across Nuclear Pores. *Cell* **171**, 1397-1410.e14 (2017).

41. Fedorchak, G. R., Kaminski, A. & Lammerding, J. Cellular mechanosensing: getting to the nucleus of it all. *Prog Biophys Mol Biol* **115**, 76–92 (2014).

42. Miroshnikova, Y. A., Nava, M. M. & Wickström, S. A. Emerging roles of mechanical forces in chromatin regulation. *Journal of Cell Science* **130**, 2243–2250 (2017).

43. Wang, N., Tytell, J. D. & Ingber, D. E. Mechanotransduction at a distance: mechanically coupling the extracellular matrix with the nucleus. *Nat Rev Mol Cell Biol* **10**, 75–82 (2009).

44. Paluch, E. K. *et al.* Mechanotransduction: use the force(s). *BMC Biol* **13**, 47 (2015).

45. Schwartz, M. A. Integrins and Extracellular Matrix in Mechanotransduction. *Cold Spring Harb Perspect Biol* **2**, a005066 (2010).

46. Yusko, E. C. & Asbury, C. L. Force is a signal that cells cannot ignore. *Mol Biol Cell* **25**, 3717–3725 (2014).

47. Provenzano, P. P. & Keely, P. J. Mechanical signaling through the cytoskeleton regulates cell proliferation by coordinated focal adhesion and Rho GTPase signaling. *J Cell Sci* **124**, 1195–1205 (2011).

48. DuFort, C. C., Paszek, M. J. & Weaver, V. M. Balancing forces: architectural control of mechanotransduction. *Nat Rev Mol Cell Biol* **12**, 308–319 (2011).

49. Engler, A. J., Sen, S., Sweeney, H. L. & Discher, D. E. Matrix elasticity directs stem cell lineage specification. *Cell* **126**, 677–689 (2006).

50. Vogel, V. & Sheetz, M. P. Cell fate regulation by coupling mechanical cycles to biochemical signaling pathways. *Curr Opin Cell Biol* **21**, 38–46 (2009).

51. Jaalouk, D. E. & Lammerding, J. Mechanotransduction gone awry. *Nat Rev Mol Cell Biol* **10**, 63–73 (2009).

52. Du, H. *et al.* Tuning immunity through tissue mechanotransduction. *Nat Rev Immunol* **23**, 174–188 (2023).

53. Weaver, V. M. *et al.* Reversion of the Malignant Phenotype of Human Breast Cells in Three-Dimensional Culture and In Vivo by Integrin Blocking Antibodies. *Journal of Cell Biology* **137**, 231–245 (1997).

54. Uhler, C. & Shivashankar, G. V. Regulation of genome organization and gene expression by nuclear mechanotransduction. *Nat Rev Mol Cell Biol* **18**, 717–727 (2017).

55. Kechagia, J. Z., Ivaska, J. & Roca-Cusachs, P. Integrins as biomechanical sensors of the microenvironment. *Nat Rev Mol Cell Biol* **20**, 457–473 (2019).

56. Hynes, R. O. Integrins: Bidirectional, Allosteric Signaling Machines. *Cell* **110**, 673–687 (2002).

57. Seetharaman, S. & Etienne-Manneville, S. Integrin diversity brings specificity in mechanotransduction. *Biol Cell* **110**, 49–64 (2018).

58. Sun, Z., Guo, S. S. & Fässler, R. Integrin-mediated mechanotransduction. *Journal of Cell Biology* **215**, 445–456 (2016).

59. Pasapera, A. M., Schneider, I. C., Rericha, E., Schlaepfer, D. D. & Waterman, C. M. Myosin II activity regulates vinculin recruitment to focal adhesions through FAK-mediated paxillin phosphorylation. *J Cell Biol* **188**, 877–890 (2010).

60. Burridge, K. & Guilluy, C. Focal adhesions, stress fibers and mechanical tension. *Exp Cell Res* **343**, 14–20 (2016).

61. De Pascalis, C. & Etienne-Manneville, S. Single and collective cell migration: the mechanics of adhesions. *MBoC* **28**, 1833–1846 (2017).

62. Harris, T. J. C. & Tepass, U. Adherens junctions: from molecules to morphogenesis. *Nat Rev Mol Cell Biol* **11**, 502–514 (2010).

63. Niessen, C. M. & Gottardi, C. J. Molecular components of the adherens junction. *Biochimica et Biophysica Acta (BBA) - Biomembranes* **1778**, 562–571 (2008).

64. Swaminathan, V. & Waterman, C. M. The molecular clutch model for mechanotransduction evolves. *Nat Cell Biol* **18**, 459–461 (2016).

65. Haining, A. W. M., von Essen, M., Attwood, S. J., Hytönen, V. P. & del Río Hernández, A. All Subdomains of the Talin Rod Are Mechanically Vulnerable and May Contribute To Cellular Mechanosensing. *ACS Nano* **10**, 6648–6658 (2016).

66. Yao, M. *et al.* Mechanical activation of vinculin binding to talin locks talin in an unfolded conformation. *Sci Rep* **4**, 4610 (2014).

67. Wang, J. Pull and push: talin activation for integrin signaling. *Cell Res* **22**, 1512–1514 (2012).

68. Kaunas, R., Nguyen, P., Usami, S. & Chien, S. Cooperative effects of Rho and mechanical stretch on stress fiber organization. *Proc Natl Acad Sci U S A* **102**, 15895–15900 (2005).

69. Saraswathibhatla, A., Indana, D. & Chaudhuri, O. Cell-extracellular matrix mechanotransduction in 3D. *Nat Rev Mol Cell Biol* **24**, 495–516 (2023).

70. Burridge, K. Focal adhesions: a personal perspective on a half century of progress. *The FEBS Journal* **284**, 3355–3361 (2017).

71. Chambliss, A. B. *et al.* The LINC-anchored actin cap connects the extracellular milieu to the nucleus for ultrafast mechanotransduction. *Sci Rep* **3**, 1087 (2013).

72. Shiu, J.-Y., Aires, L., Lin, Z. & Vogel, V. Nanopillar force measurements reveal actin-cap-mediated YAP mechanotransduction. *Nat Cell Biol* **20**, 262–271 (2018).

73. Maninová, M. & Vomastek, T. Dorsal stress fibers, transverse actin arcs, and perinuclear actin fibers form an interconnected network that induces nuclear movement in polarizing fibroblasts. *The FEBS Journal* **283**, 3676–3693 (2016).

74. Miroshnikova, Y. A. & Wickström, S. A. Mechanical Forces in Nuclear Organization. *Cold Spring Harb Perspect Biol* **14**, a039685 (2022).

75. Kim, J.-K. *et al.* Nuclear lamin A/C harnesses the perinuclear apical actin cables to protect nuclear morphology. *Nat Commun* **8**, 2123 (2017).

76. Lombardi, M. L. *et al.* The Interaction between Nesprins and Sun Proteins at the Nuclear Envelope Is Critical for Force Transmission between the Nucleus and Cytoskeleton. *J Biol Chem* **286**, 26743–26753 (2011).

77. Sosa, B. A., Rothballer, A., Kutay, U. & Schwartz, T. U. LINC Complexes Form by Binding of Three KASH Peptides to the Interfaces of Trimeric SUN proteins. *Cell* **149**, 1035–1047 (2012).

78. Jahed, Z., Soheilypour, M., Peyro, M. & Mofrad, M. R. K. The LINC and NPC relationship - it's complicated! *J Cell Sci* **129**, 3219–3229 (2016).

79. Li, P. & Noegel, A. A. Inner nuclear envelope protein SUN1 plays a prominent role in mammalian mRNA export. *Nucleic Acids Res* **43**, 9874–9888 (2015).

80. Lammerding, J. Mechanics of the Nucleus. *Compr Physiol* **1**, 783–807 (2011).

81. Kirby, T. J. & Lammerding, J. Emerging views of the nucleus as a cellular mechanosensor. *Nat Cell Biol* **20**, 373–381 (2018).

82. Kalukula, Y., Stephens, A. D., Lammerding, J. & Gabriele, S. Mechanics and functional consequences of nuclear deformations. *Nat Rev Mol Cell Biol* **23**, 583–602 (2022).

83. Xie, W. *et al.* A-type Lamins Form Distinct Filamentous Networks with Differential Nuclear Pore Complex Associations. *Current Biology* **26**, 2651–2658 (2016).

84. Guilluy, C. *et al.* Isolated nuclei adapt to force and reveal a mechanotransduction pathway in the nucleus. *Nat Cell Biol* **16**, 376–381 (2014).

85. Ghagre, A., Delarue, A., Srivastava, L. K., Koushki, N. & Ehrlicher, A. Nuclear curvature determines Yes-associated protein localization and differentiation of mesenchymal stem cells. *Biophysical Journal* **123**, 1222–1239 (2024).

86. Szczesny, S. E. & Mauck, R. L. The Nuclear Option: Evidence Implicating the Cell Nucleus in Mechanotransduction. *J Biomech Eng* **139**, 0210061–02100616 (2017).

87. Lammerding, J. *et al.* Abnormal nuclear shape and impaired mechanotransduction in emerin-deficient cells. *J Cell Biol* **170**, 781–791 (2005).

88. Boyden, E. S., Zhang, F., Bamberg, E., Nagel, G. & Deisseroth, K. Millisecond-timescale, genetically targeted optical control of neural activity. *Nat Neurosci* **8**, 1263–1268 (2005).

89. Jayaraman, P. *et al.* Blue light-mediated transcriptional activation and repression of gene expression in bacteria. *Nucleic Acids Res* **44**, 6994–7005 (2016).

90. Zhang, K. & Cui, B. Optogenetic control of intracellular signaling pathways. *Trends Biotechnol* **33**, 92–100 (2015).

91. Steinbeck, J. A. *et al.* Optogenetics enables functional analysis of human embryonic stem cell-derived grafts in a Parkinson's disease model. *Nat Biotechnol* **33**, 204–209 (2015).

92. Nussinovitch, U. & Gepstein, L. Optogenetics for in vivo cardiac pacing and resynchronization therapies. *Nat Biotechnol* **33**, 750–754 (2015).

93. Mühlhäuser, W. W. D., Fischer, A., Weber, W. & Radziwill, G. Optogenetics - Bringing light into the darkness of mammalian signal transduction. *Biochimica et Biophysica Acta (BBA) - Molecular Cell Research* **1864**, 280–292 (2017).

94. Bonger, K. M., Rakhit, R., Payumo, A. Y., Chen, J. K. & Wandless, T. J. General method for regulating protein stability with light. *ACS Chem Biol* **9**, 111–115 (2014).

95. Crefcoeur, R. P., Yin, R., Ulm, R. & Halazonetis, T. D. Ultraviolet-B-mediated induction of protein-protein interactions in mammalian cells. *Nat Commun* **4**, 1779 (2013).

96. Beyer, H. M. *et al.* Red Light-Regulated Reversible Nuclear Localization of Proteins in Mammalian Cells and Zebrafish. *ACS Synth Biol* **4**, 951–958 (2015).

97. Niopek, D. *et al.* Engineering light-inducible nuclear localization signals for precise spatiotemporal control of protein dynamics in living cells. *Nat Commun* **5**, 4404 (2014).

98. Yumerefendi, H. *et al.* Light-induced nuclear export reveals rapid dynamics of epigenetic modifications. *Nat Chem Biol* **12**, 399–401 (2016).

99. Hemphill, J., Borchardt, E. K., Brown, K., Asokan, A. & Deiters, A. Optical Control of CRISPR/Cas9 Gene Editing. *J Am Chem Soc* **137**, 5642–5645 (2015).

100. Kichuk, T. C., Carrasco-López, C. & Avalos, J. L. Lights up on organelles: Optogenetic tools to control subcellular structure and organization. *WIREs Mech Dis* **13**, e1500 (2021).

101. Repina, N. A., Rosenbloom, A., Mukherjee, A., Schaffer, D. V. & Kane, R. S. At Light Speed: Advances in Optogenetic Systems for Regulating Cell Signaling and Behavior. *Annu Rev Chem Biomol Eng* **8**, 13–39 (2017).

102. Icha, J., Weber, M., Waters, J. C. & Norden, C. Phototoxicity in live fluorescence microscopy, and how to avoid it. *BioEssays* **39**, 1700003 (2017).

103. Tischer, D. & Weiner, O. D. Illuminating cell signalling with optogenetic tools. *Nat Rev Mol Cell Biol* **15**, 551–558 (2014).

104. Forlani, G. *et al.* Analysis of Slow-Cycling Variants of the Light-Inducible Nuclear Protein Export System LEXY in Mammalian Cells. *ACS Synth. Biol.* **11**, 3529–3533 (2022).

105. Hoffman, L. M. *et al.* Mechanical stress triggers nuclear remodeling and the formation of transmembrane actin nuclear lines with associated nuclear pore complexes. *MBoC* **31**, 1774–1787 (2020).

106. Yang, Z. *et al.* The destruction of cytoplasmic skeleton leads to the change of nuclear structure and the looseness of lamin A submicroscopic network. *Heliyon* **10**, e36583 (2024).

107. Neelam, S., Hayes, P. R., Zhang, Q., Dickinson, R. B. & Lele, T. P. Vertical uniformity of cells and nuclei in epithelial monolayers. *Sci Rep* **6**, 19689 (2016).

108. Ihalainen, T. O. *et al.* Differential basal-to-apical accessibility of lamin A/C epitopes in the nuclear lamina regulated by changes in cytoskeletal tension. *Nat Mater* **14**, 1252–1261 (2015).

109. Kögler, A. C. *et al.* Extremely rapid and reversible optogenetic perturbation of nuclear proteins in living embryos. *Dev Cell* **56**, 2348-2363.e8 (2021).

110. Timney, B. L. *et al.* Simple kinetic relationships and nonspecific competition govern nuclear import rates in vivo. *J Cell Biol* **175**, 579–593 (2006).

111. Wang, N., Tytell, J. D. & Ingber, D. E. Mechanotransduction at a distance: mechanically coupling the extracellular matrix with the nucleus. *Nat Rev Mol Cell Biol* **10**, 75–82 (2009).

112. Kassianidou, E., Kalita, J. & Lim, R. Y. H. The role of nucleocytoplasmic transport in mechanotransduction. *Experimental Cell Research* **377**, 86–93 (2019).

113. Scott, K. L. *et al.* Nucleocytoplasmic transport rates are regulated by cellular processes that modulate GTP availability. *Journal of Cell Biology* **223**, e202308152 (2024).

114. Swaminathan, V. *et al.* Mechanical Stiffness Grades Metastatic Potential in Patient Tumor Cells and in Cancer Cell Lines. *Cancer Research* **71**, 5075–5080 (2011).

115. Chiotaki, R., Polioudaki, H. & Theodoropoulos, P. A. Differential nuclear shape dynamics of invasive andnon-invasive breast cancer cells are associated with actin cytoskeleton organization and stability. *Biochem. Cell Biol.* **92**, 287–295 (2014).

116. Gil-Redondo, J. C., Weber, A., Zbiral, B., Vivanco, M. dM. & Toca-Herrera, J. L. Substrate stiffness modulates the viscoelastic properties of MCF-7 cells. *Journal of the Mechanical Behavior of Biomedical Materials* **125**, 104979 (2022).

117. Bell, E. S. *et al.* Low lamin A levels enhance confined cell migration and metastatic capacity in breast cancer. *Oncogene* **41**, 4211–4230 (2022).

118. Pemberton, L. F. & Paschal, B. M. Mechanisms of Receptor-Mediated Nuclear Import and Nuclear Export. *Traffic* **6**, 187–198 (2005).